Data report: consolidation characteristics of sediments from IODP Expedition 308, Ursa Basin, Gulf of Mexico[1]

H. Long,[2,3] P.B. Flemings,[4] J.T. Germaine,[5] D.M. Saffer,[6] and B. Dugan[7]

Chapter contents

[1] Long, H., Flemings, P.B., Germaine, J.T., Saffer, D.M., and Dugan, B., 2008. Data report: consolidation characteristics of sediments from IODP Expedition 308, Ursa Basin, Gulf of Mexico. *In* Flemings, P.B., Behrmann, J.H., John, C.M., and the Expedition 308 Scientists, *Proc. IODP,* 308: College Station, TX (Integrated Ocean Drilling Program Management International, Inc.). doi:10.2204/iodp.proc.308.204.2008
[2] Department of Energy and Mineral Engineering, The Pennsylvania State University, University Park PA 16802, USA.
[3] Present address: ExxonMobil Upstream Research Company, Houston, TX 77098.
[4] John A. and Katherine G. Jackson School of Geosciences, The University of Texas at Austin, Austin TX 78712, USA. pflemings@jsg.utexas.edu
[5] Department of Civil and Environmental Engineering, Massachusetts Institute of Technology, Cambridge MA 02139, USA.
[6] Department of Geosciences, The Pennsylvania State University, University Park, PA 16802, USA.
[7] Department of Earth Science, Rice University, Houston TX 77005, USA.

Abstract

We conducted constant rate of strain consolidation tests on 9 samples from Integrated Ocean Drilling Program Site U1322 and 23 samples from Site U1324 in three laboratories (Massachusetts Institute of Technology, Pennsylvania State University, and Rice University) to obtain the consolidation properties of the sediment, as well as determine the stress history of the sites. The sediments recovered from above 200 meters below seafloor (mbsf) at both sites have similar consolidation properties. The compression index (C_c) ranges from 0.1508 to 0.5052. C_c decreases with void ratio at both sites. The expansion index (C_e) ranges from 0.0153 to 0.1144 and decreases with void ratio at both sites. The in situ hydraulic conductivity (K_i) ranges from 2.18×10^{-11} to 6.38×10^{-10} m/s. K_i decreases with depth. The e-log(K_i) relation has different slopes for sediments above and below 300 mbsf at Site U1324. The coefficient of consolidation (c_v) ranges from 1.5×10^{-8} to 4.2×10^{-7} m^2/s. c_v increases with depth for the sediments above 200 mbsf at both sites and shows no clear trend for the sediments below 200 mbsf at Site U1324. The preconsolidation pressure (P'_c) is significantly less than the hydrostatic vertical effective stress (σ'_{vh}) at both sites, which suggests that Ursa sediments are overpressured.

Introduction

Understanding overpressure, fluid flow, and sediment compression behavior is critical for evaluating the stability of continental slopes. Integrated Ocean Drilling Program (IODP) Expedition 308 was aimed at testing a multidimensional flow model by examining how physical properties, pressure, temperature, and pore fluid composition vary within low-permeability mudstones that overlie a permeable and overpressured aquifer (see the **"Expedition 308 summary"** chapter). We drilled, logged, cored, and made in situ measurements in a region of very rapid Pleistocene sedimentation: the Ursa Basin (Fig. **F1**).

We took whole-core geotechnical samples for shore-based consolidation tests (Table **T1**). Consolidation tests simulate how porosity evolves with effective stress under one-dimensional gravitational compaction caused by sedimentation. The transition from recompression to virgin compression behavior provides an estimate of the maximum in situ effective stress the sample has undergone

doi:10.2204/iodp.proc.308.204.2008

(Becker et al., 1987; Casagrande, 1936). The experiments also provide insight into how permeability evolves with burial and compression.

Consolidation properties were determined from results of constant rate of strain consolidation (CRSC) tests on intact samples.

Laboratory testing methodology

Sample handling and preparation

The coring techniques include the advanced piston corer (APC) and extended core barrel (XCB) systems (Table T1). These standard coring systems and their characteristics are summarized in *Technical Note* 31 of the Ocean Drilling Program (Graber et al., 2002). The sample was not extruded from the core liner on board the drilling ship. Whole-core samples were capped and sealed in wax to maintain natural saturation during refrigerated storage prior to the experiments. For the experiments, each sample was removed from the wax-sealed liner and subsampled with a sharp cutting shoe (at Pennsylvania State University [PSU]) or a trimming jig (at Massachusetts Institute of Technology [MIT] and Rice University [Rice]).

Sample descriptions

Table T1 illustrates all of the samples tested in this study including sample depth, type of coring used to acquire the sample, what analyses were done, and where the analyses were done. Most of the PSU and MIT samples were X-rayed at MIT's radiography facility in order to select undisturbed portions of the core for experiments and to assess the presence of inclusions and variation in fabric. The Rice samples were X-rayed by Fugro in order to select undisturbed portions for experiments and to identify layering or inhomogeneities. Core X-ray data can be found in H. Nelson et al. (unpubl. data).

All samples were taken from whole core, not core catchers. Sample locations are illustrated in Table T1. Quality of samples generally decreases with depth and many samples had significant deformation caused by the coring process. Table T1 indicates which samples were recovered by the APC and XCB systems. During APC coring, two different cutting shoes were used: the "Fugro" cutting shoe and the "IODP-APC" cutting shoe. The Fugro cutting shoe has a thinner kerf than the IODP-APC cutting shoe; therefore, less deformation during coring was expected.

Grain size analysis documents that all tested samples are silty clays containing 50%–70% clay-sized grains (<2 µm), except samples from Section 308-U1324C-7H-1 (405 meters below seafloor [mbsf]), which are clayey silt with 30% clay-sized grains (**Sawyer et al.,** this volume). The mineralogic composition of the silty clay samples is similar. Quantitative X-ray mineralogy shows that illite and smectite are the dominant minerals and together comprise 37%–60% of the bulk rock weight. Analysis of the clay-sized fraction (<2 µm) by subjective analysis of oriented mounts shows that 80%–90% of the mixed-layer interlayers are composed of smectite.

Index properties

Two water contents were measured in the consolidation test: w_c and w_n. w_c is the water content measured on the leftover trimmings during sample preparation. w_n is the water content measured on the test specimen itself. We measured the water content by oven-drying the samples. Water content is calculated by taking the difference in the weight of the sample before and after oven-drying and dividing this difference by the oven-dried weight.

In the laboratory, water content was measured on the trimmings from the specimens and on the specimens themselves. The water content of the trimmings were generally lower (~3%) than the water content of the samples. We compared the water content measured on the specimens with the shipboard measurements of moisture and density (MAD). This comparison is difficult because the sampling frequency and quality of the MAD data are variable. We find that at 15 locations the difference between the laboratory-derived water content and the MAD measurements are within 5 units in water content. There is no systematic difference.

Constant rate of strain consolidation testing

CRSC tests were conducted at three laboratories (MIT, PSU, and Rice) in general accordance with American Society for Testing and Materials (ASTM) D4186 guidelines (ASTM International, 2006). As the name implies, during CRSC tests the sample is deformed at a constant strain rate. This has several advantages relative to traditional step-loading tests. It provides continuous loading data, which provide a much more detailed view of compression behavior. In contrast with incremental loading, data points are obtained by doubling stress levels: behavior must be inferred between these points. In addition, continuous measurements of the flow properties are obtained (both the hydraulic conductivity [K] and the coefficient of consolidation [c_v]). Finally, K is calculated directly (Equation 2), as opposed to the incremental consolidation test where it is indirectly

calculated from the coefficient of consolidation (c_v) and the frame compressibility (m_v).

The dimensions of the specimen are slightly different between the three laboratories. MIT specimens were 5.95–6.35 cm in diameter with an initial height of 2.35 cm. PSU specimens were 5 cm in diameter with an initial height of 2.0 cm. Rice specimens were 5.09 cm in diameter with an initial height of 2.41 cm.

Specimens were laterally confined with a steel ring. Prior to testing, specimens were saturated with de-aired distilled water and back-pressured to 300–425 kPa for 24 h to drive any gases present into solution. We applied a constant rate of strain using a computer-controlled load frame, with the sample base undrained and sample top open to the backpressure. We continuously monitored sample height (H, in millimeters), applied vertical stress (σ_v, in kPa), and basal pore pressure (u, in kPa). At PSU, an axial load of 50 kN could be applied by a mechanical load frame and 5 cm diameter samples were run; therefore, the maximum vertical stress was 25.5 MPa. Backpressure was 0.3 MPa; therefore, the maximum effective stress that could be achieved was ~25.2 MPa. The MIT and Rice apparatuses were capable of lower total effective stresses. Most MIT experiments were run to ~2 MPa. Most Rice experiments were completed at effective stresses near 4 MPa. For this reason, the MIT and Rice apparatuses were used on the shallower samples.

The vertical effective stress (σ'_v), hydraulic conductivity (K), compressibility (m_v), coefficient of consolidation (c_v), and strain energy density (SED) were calculated using the following equations (ASTM, 2006; Tan et al., 2006):

$$\sigma'_v = \sigma_v - \frac{2}{3} \cdot \Delta u\,, \tag{1}$$

$$K = \frac{\frac{d\varepsilon}{dt} \cdot H_0 \cdot H \cdot \gamma_w}{2 \cdot \Delta u}, \tag{2}$$

$$m_v = \frac{\Delta\varepsilon}{\Delta\sigma'_v}, \tag{3}$$

$$c_v = \frac{K}{m_v \cdot \gamma_w}\,, \text{and} \tag{4}$$

$$\text{SED} = \frac{\sigma'_{v_{i-1}} + \sigma'_{v_i}}{2} \cdot Ln\left(\frac{1-\varepsilon_{i-1}}{1-\varepsilon_i}\right). \tag{5}$$

Variables are defined in Table **T2.**

Laboratory testing results

We conducted CRSC tests on 9 samples from Site U1322 and 23 samples from Site U1324 in two laboratories (MIT and PSU). Table **T3** summarizes the details of each CRSC test. Figures **F4, F5, F6, F7, F8, F9, F10, F11, F12, F13, F14, F15, F16, F17, F18, F19, F20, F21, F22, F23, F24, F25, F26, F27, F28, F29, F30, F31, F32, F33, F34,** and **F35** show the consolidation curves in both e-log (σ'_v) and ε-log (σ'_v), normalized excess pore pressure, coefficient of consolidation (c_v), SED, and hydraulic conductivity (K) for each CRSC test. The CRSC data sheet, which includes 12 columns (Table **T4**), can be found in Microsoft Excel format in **"Supplementary material."**

The compression index (C_c) refers to the slope of the normally consolidated portion of the compression curve in e-log (σ'_v) space (Fig. **F2**). The compression behavior of the samples is similar at Sites U1322 and U1324 (Fig. **F36**). The measured values of c_c range from 0.1508 to 0.5052. c_c decreases with void ratio at both sites (Fig. **F36**). The expansion index (c_e) refers to the slope of the unloading portion of the compression curve in e-log (σ'_v) space. It ranges from 0.0153 to 0.1144 and also decreases with void ratio (Fig. **F36**). It must be noted that the expansion index varies with the amount of unloading that occurs. As such, the quoted expansion indexes are for unloading to an overconsolidation ratio of 10.

The in situ hydraulic conductivity (K_i) is obtained by extrapolating the linear portion of the e-log(K) relation to the in situ void ratio. Values of K_i range from 2.18×10^{-11} to 6.38×10^{-10} m/s. K_i decreases with depth (Fig. **F37**). The e_i-log(K_i) relations for sediments above and below 300 mbsf have different slopes (Fig. **F37**). K_i of the clayey silt sample (405.81 mbsf) is significantly higher than those of the silty clay samples, which reflects the lithology difference and stands out on the e_i-log(K_i) plot (Fig. **F37**).

The coefficient of consolidation, c_v, ranges from 1.5×10^{-8} to 4.2×10^{-7} m²/s (Fig. **F38**). c_v increases with depth for the sediments above 200 mbsf at both sites and shows no clear trend for the sediments below 200 mbsf. c_v of the clayey silt sample (405.81 mbsf) is significantly higher than those of the silty clay samples, which reflects the lithology difference.

The preconsolidation pressure, P'_c, is determined using the work-stress method proposed by Becker et al. (1987). Figure **F3** illustrates this approach for one sample (CRS802). P'_c is significantly less than the hydrostatic vertical effective stress (σ'_{vh}) at both sites (Fig. **F39**), which suggests that Ursa sediments are overpressured.

Acknowledgments

This research used samples provided by the Integrated Ocean Drilling Program (IODP). Funding for this research was provided by the U.S. Science Support Program for IODP that is administered by Joint Oceanographic Institutions (now renamed Consortium for Ocean Leadership). In addition, U.S. National Science Foundation Grants 0447235 and 0351085 supported this research. This research was also sponsored by the Petroleum Research Fund (PRF# 44476-AC8).

References

ASTM International, 2006. Standard test method for one-dimensional consolidation properties of saturated cohesive soils using controlled-strain loading (Standard D4186-06). In *Annual Book of ASTM Standards* (Vol. 04.08): *Soil and Rock* (I): West Conshohocken, PA (Am. Soc. Testing and Mater.)

Becker, D.E., Crooks, J.H.A., Been, K., and Jeffries, M.G., 1987. Work as a criterion for determining in situ and yield stresses in clays. *Can. Geotech. J.,* 24(4):549–564.

Casagrande, A., 1936. The determination of pre-consolidation load and its practical significance. *In* Casagrande, A., Rutledge, P.C., and Watson, J.D. (Eds.)*, Proc. 1st Int. Conf. Soil Mech. Found. Eng.* Am. Soc. Civ. Eng., 3:60–64.

Graber, K.K., Pollard, E., Jonasson, B., and Schulte, E. (Eds.), 2002. Overview of Ocean Drilling Program Engineering Tools and Hardware. *ODP Tech. Note,* 31. **doi:10.2973/odp.tn.31.2002**

Tan, B., Germaine, J.T., and Flemings, P.B., 2006. Data report: consolidation and strength characteristics of sediments from ODP Site 1244, Hydrate Ridge, Cascadia continental margin. *In* Tréhu, A.M., Bohrmann, G., Torres, M.E., and Colwell, F.S. (Eds.), *Proc. ODP, Sci. Results,* 204: College Station, TX (Ocean Drilling Program), 1–148. **doi:10.2973/odp.proc.sr.204.102.2006**

Initial receipt: 22 June 2007
Acceptance: 31 January 2008
Publication: 1 July 2008
MS 308-204

Figure F1. A. IODP Expedition 308 site locations (red circles) and bathymetry contours. Ursa Basin is located 210 km southeast of New Orleans, Louisiana, USA (inset map). Contour interval = 100 m. **B.** East–west seismic cross section A–A′ (located in A). VE = vertical exaggeration. **C.** Interpreted cross section A–A′. Light and dark gray = mud-rich levee, rotated channel-margin slides, and hemipelagic drape; yellow = sand-rich channel fill. Blue Unit (light blue) composed of sand and mud. Mass transport deposits (MTDs) have occurred in the mud-rich levee deposits above the Blue Unit. Red = detachment surfaces.

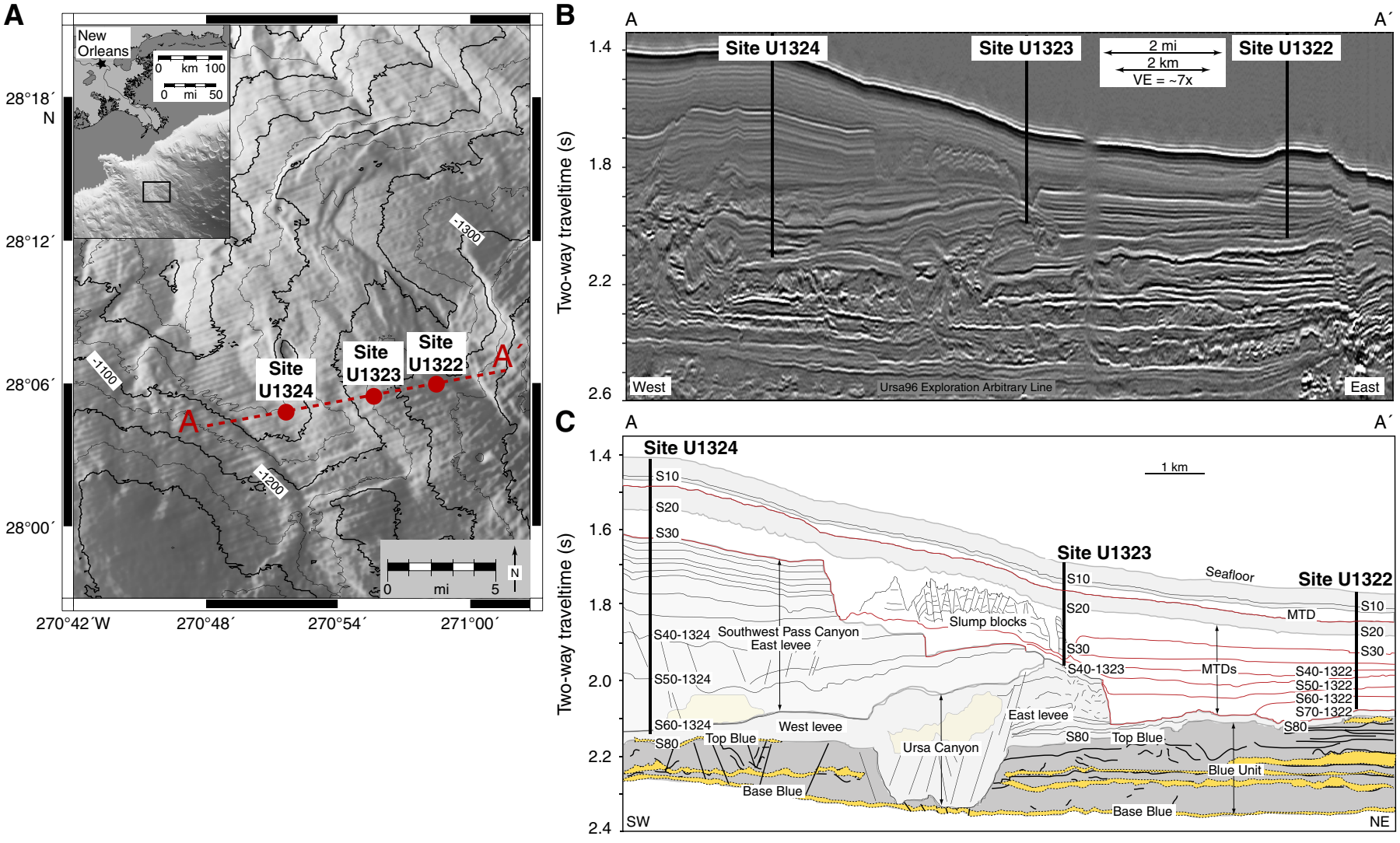

Figure F2. Examples of consolidation test results. σ'_{vh} = hydrostatic vertical effective stress calculated from LWD bulk density profile and assumed seawater density of 1.024 g/cm^3. Preconsolidation pressures (P'_c, open circle) derived using work-stress method (Becker et al., 1987).

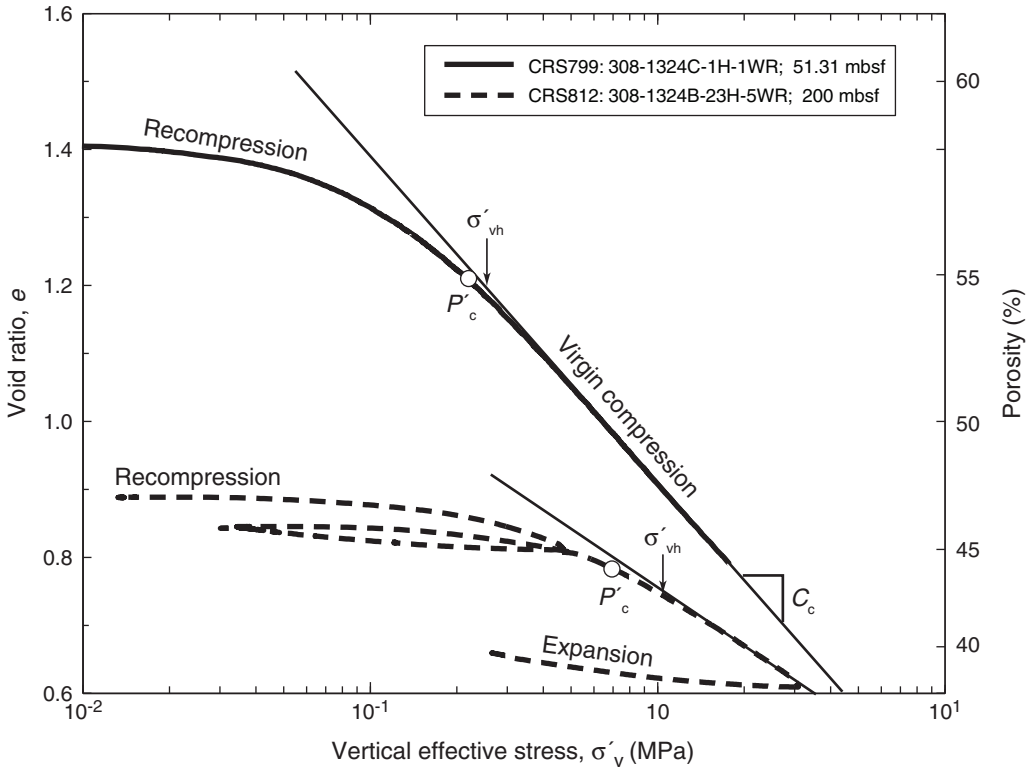

Figure F3. Derivation of preconsolidation pressure using work-stress method of Becker et al. (1987) based on data from CRS802.

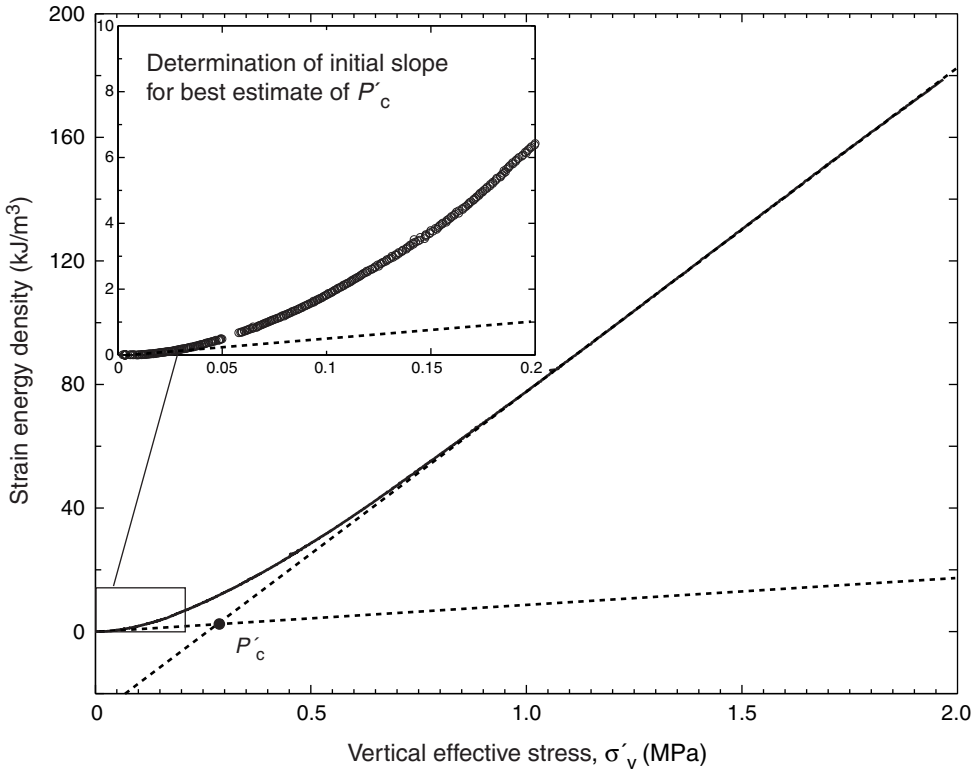

Figure F4. CRS796 consolidation data for Sample 308-U1322D-2H-2WR, 72.78 mbsf. Coef. = coefficient.

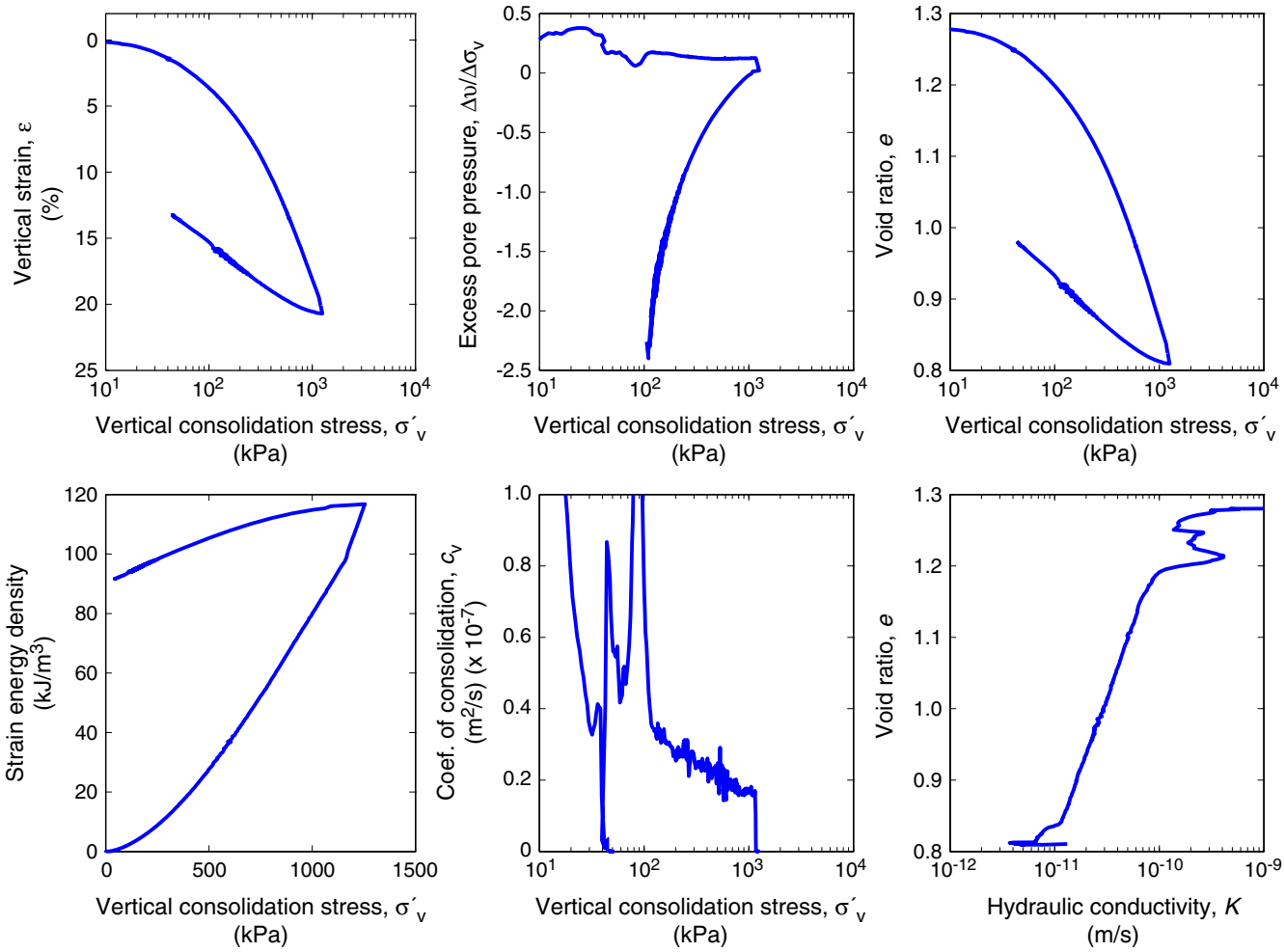

Figure F5. CRS797 consolidation data for Sample 308-U1324C-1H-1WR, 51.27 mbsf. Coef. = coefficient.

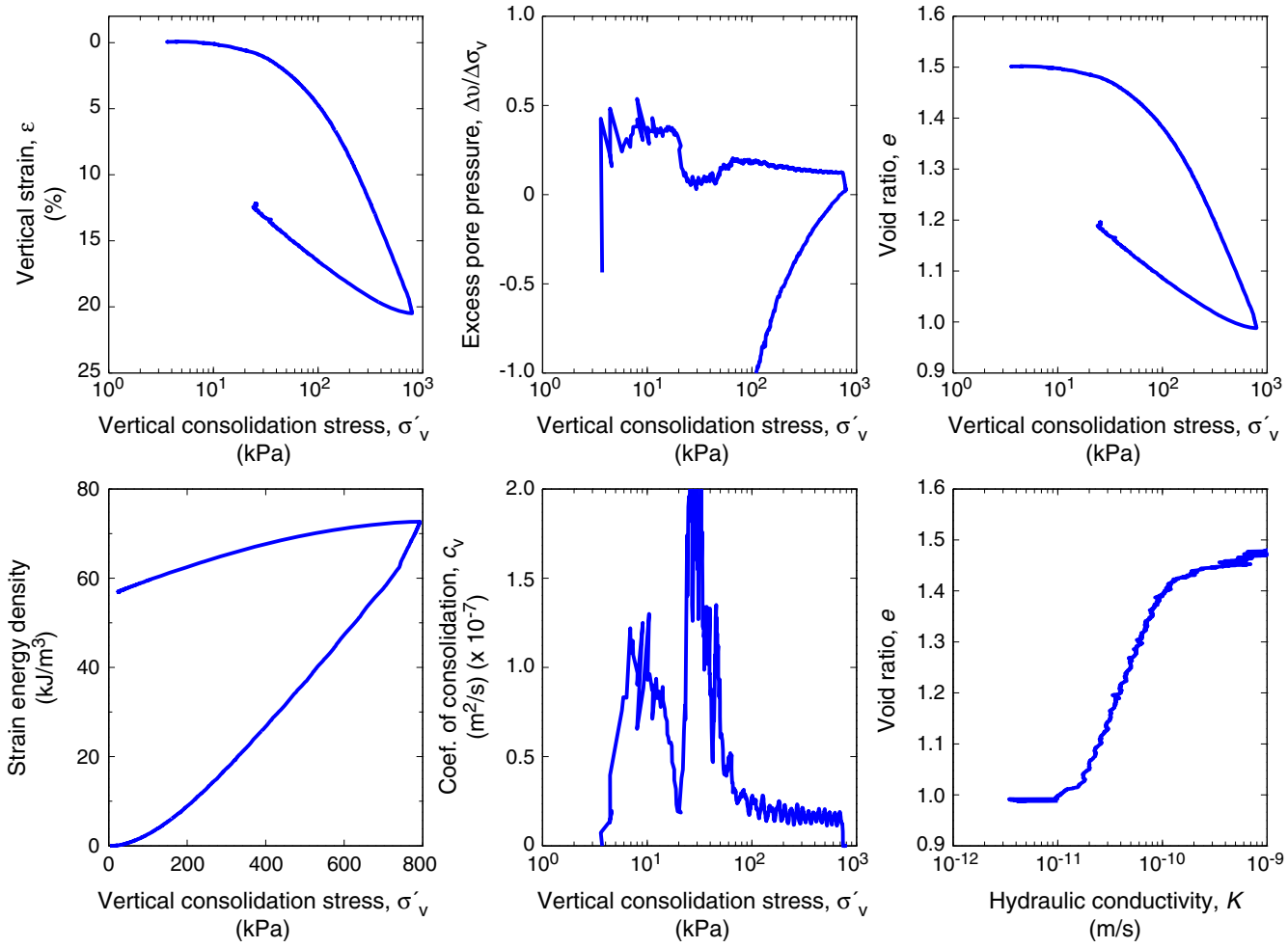

Figure F6. CRS798 consolidation data for Sample 308-U1322D-2H-2WR, 72.83 mbsf. Coef. = coefficient.

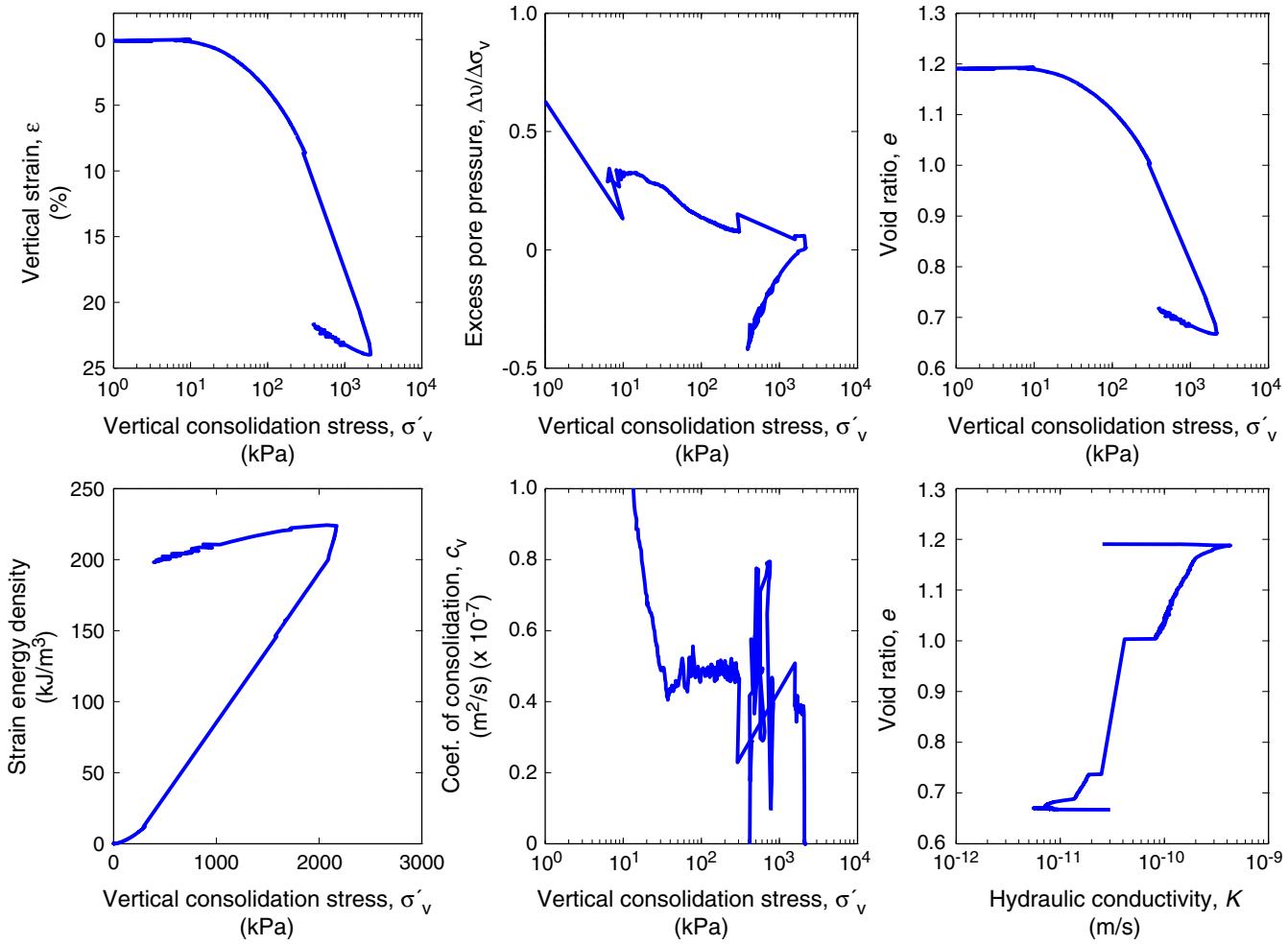

Figure F7. CRS799 consolidation data for Sample 308-U1324C-1H-1WR, 51.31 mbsf. Coef. = coefficient.

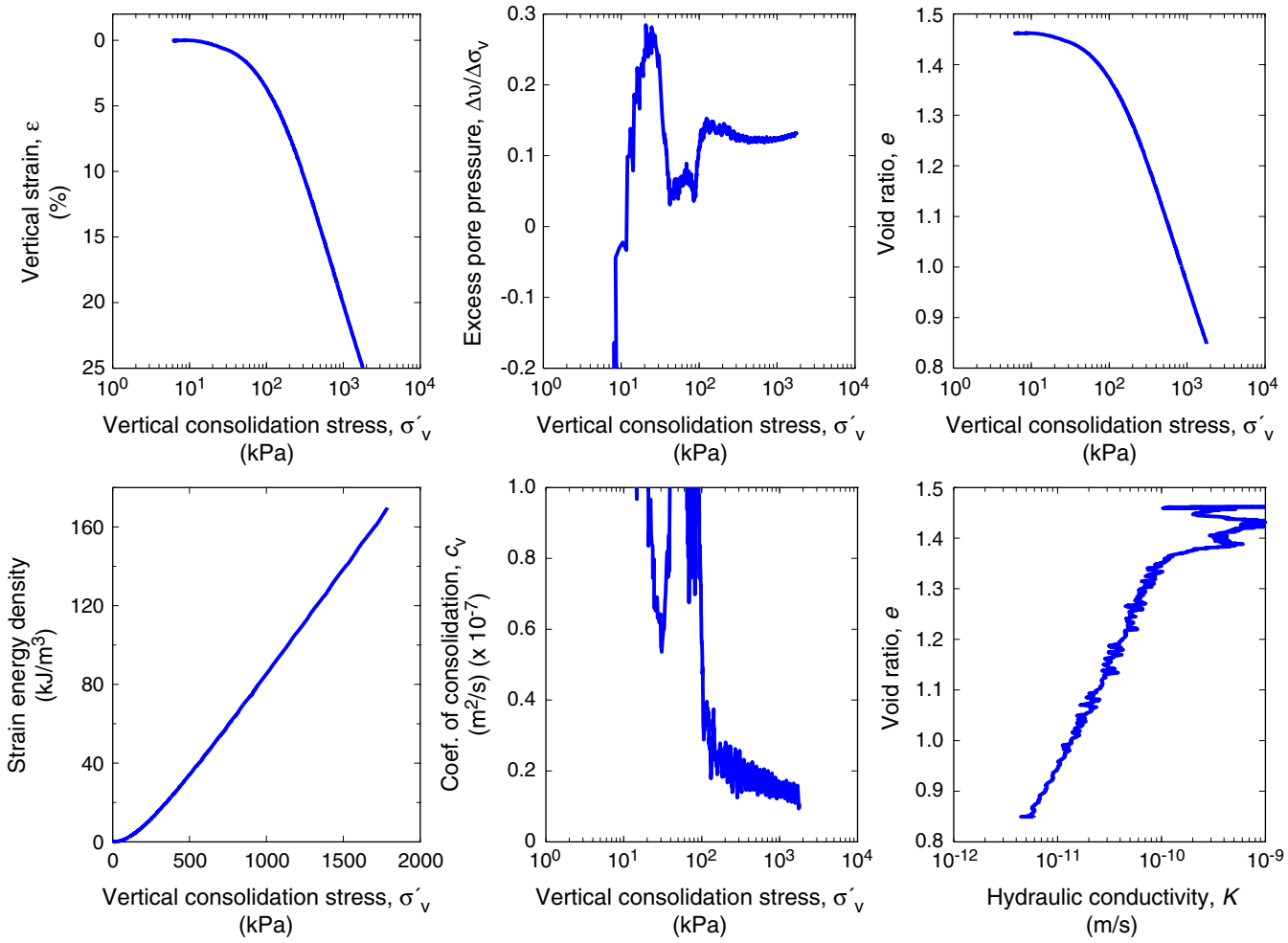

Figure F8. CRS800 consolidation data for Sample 308-U1324B-4H-7WR, 31.86 mbsf. Coef. = coefficient.

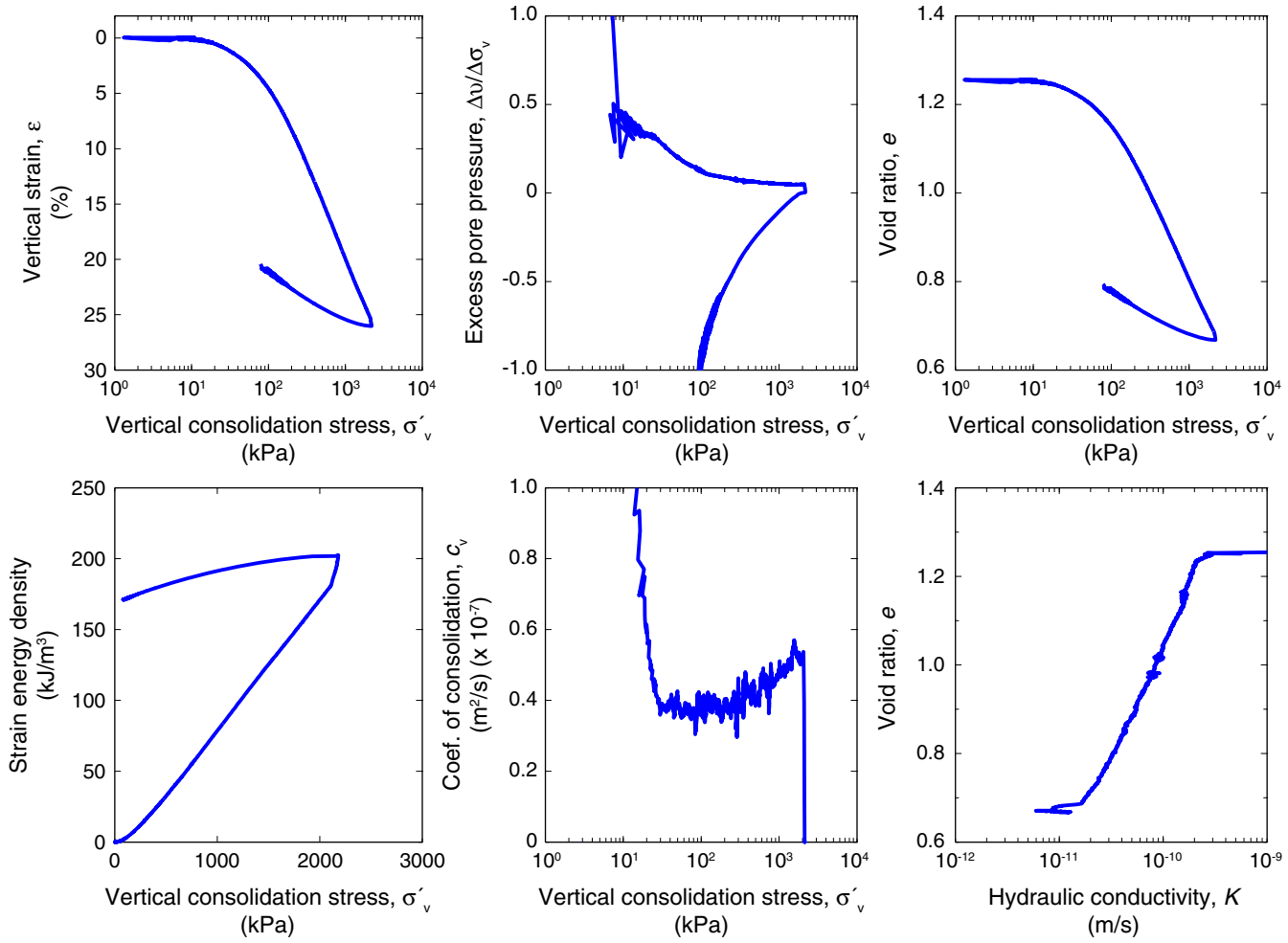

Figure F9. CRS801 consolidation data for Sample 308-U1324B-16H-5WR, 142.13 mbsf. Coef. = coefficient.w

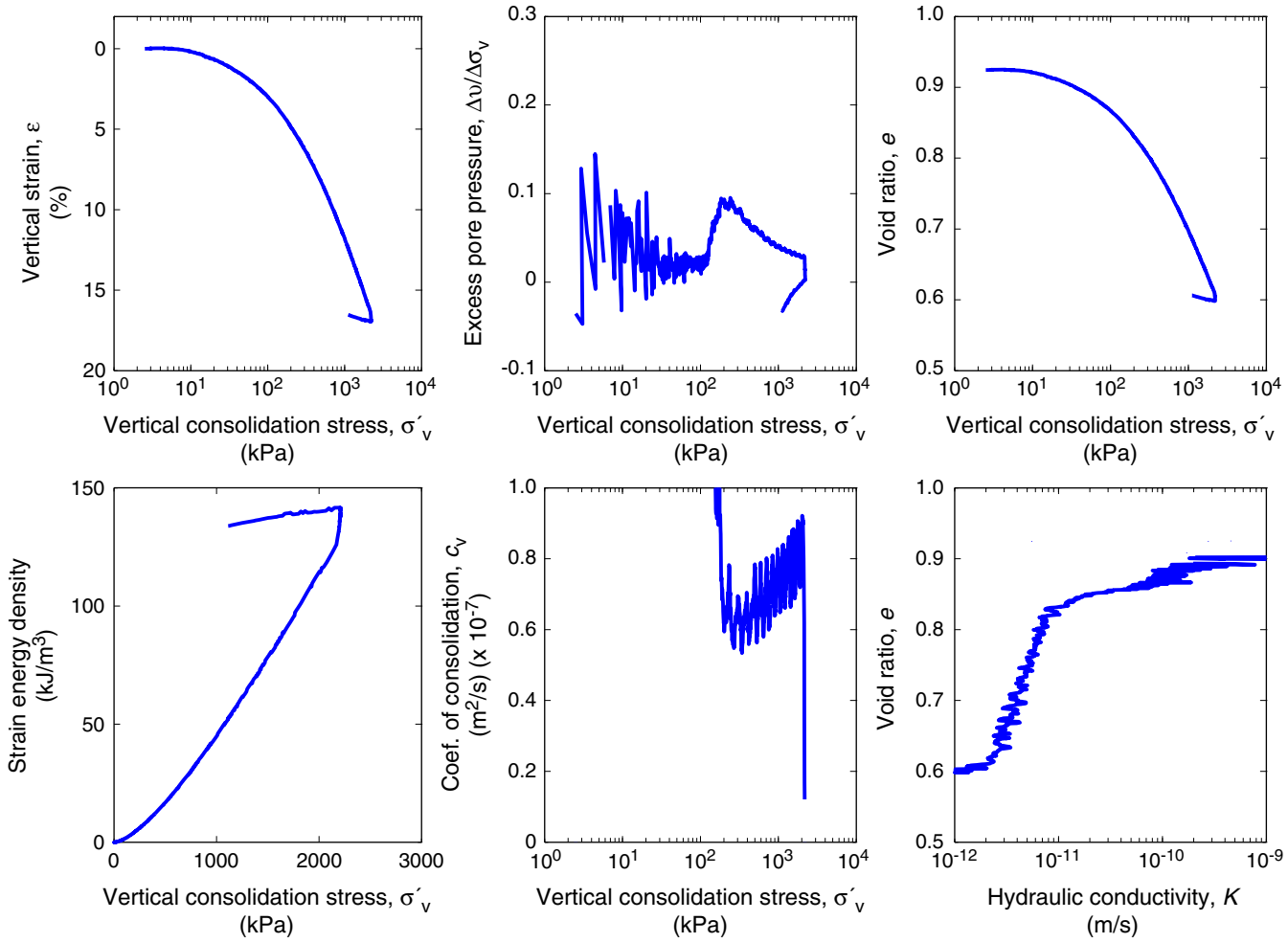

Figure F10. CRS802 consolidation data for Sample 308-U1324B-7H-7WR, 60.31 mbsf. Coef. = coefficient.

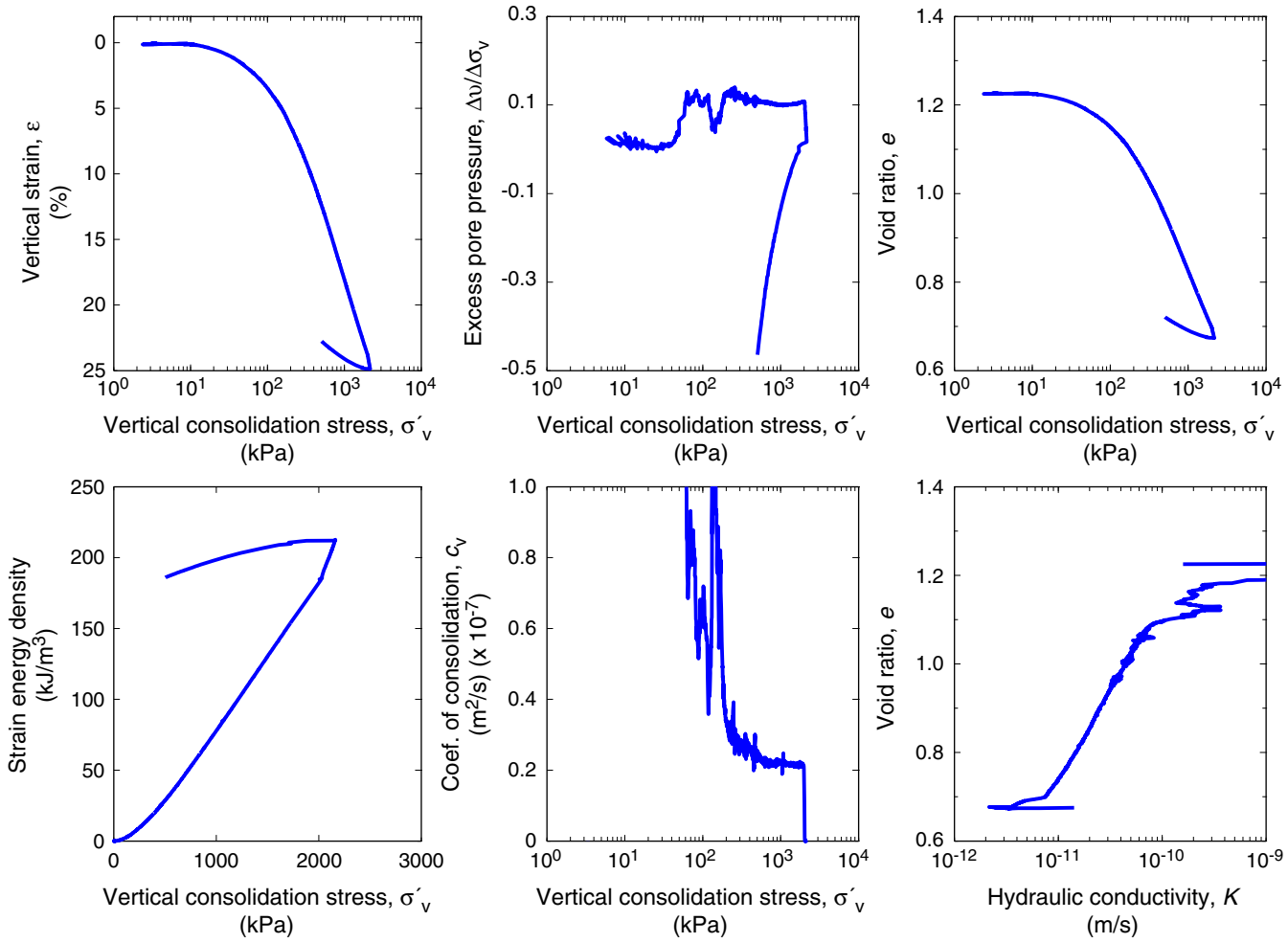

Figure F11. CRS803 consolidation data for Sample 308-U1324B-15H-5WR, 134.2 mbsf. Coef. = coefficient.

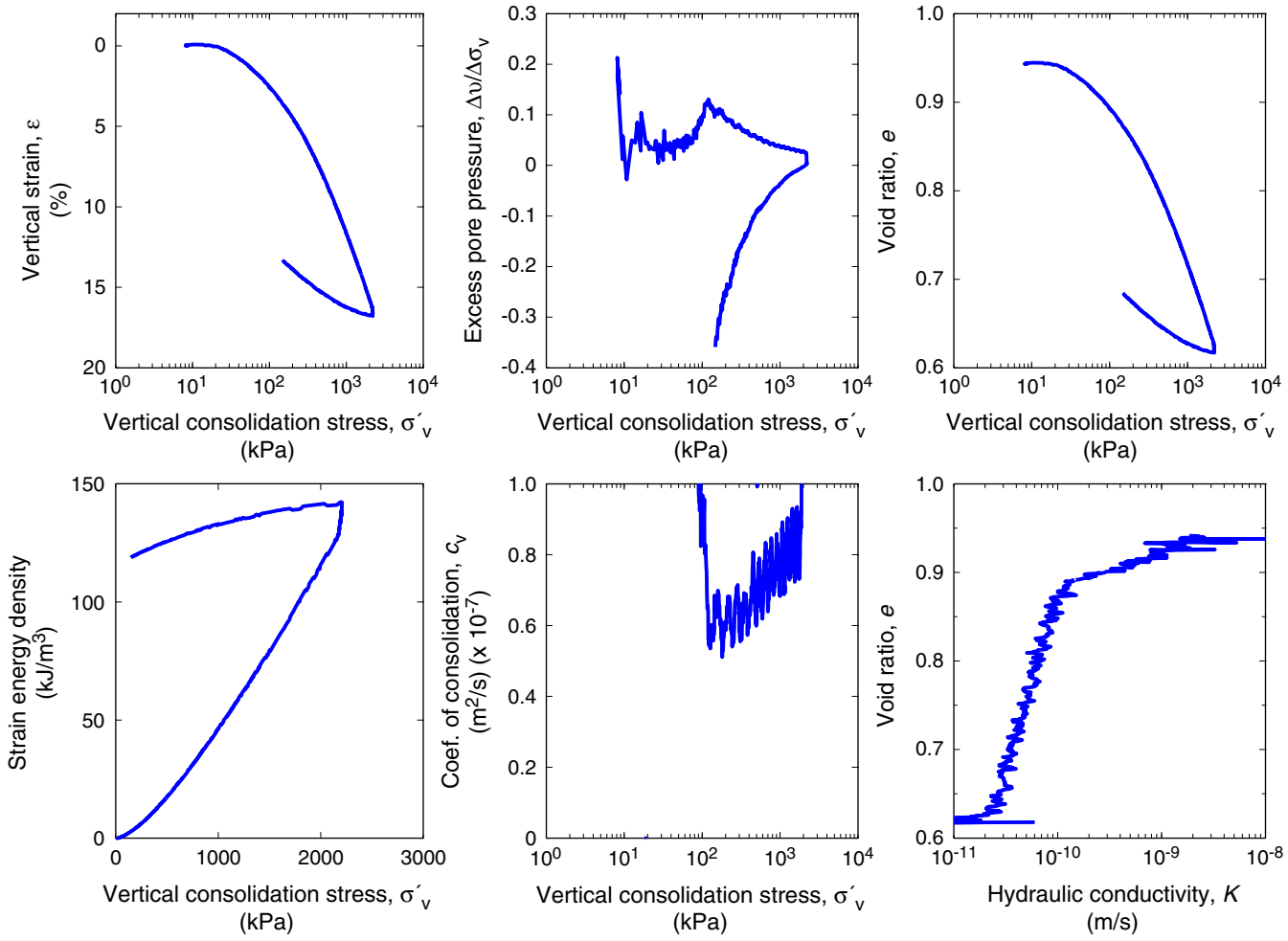

Figure F12. CRS807 consolidation data for Sample 308-U1324C-2H-4WR, 105.48 mbsf. Coef. = coefficient.

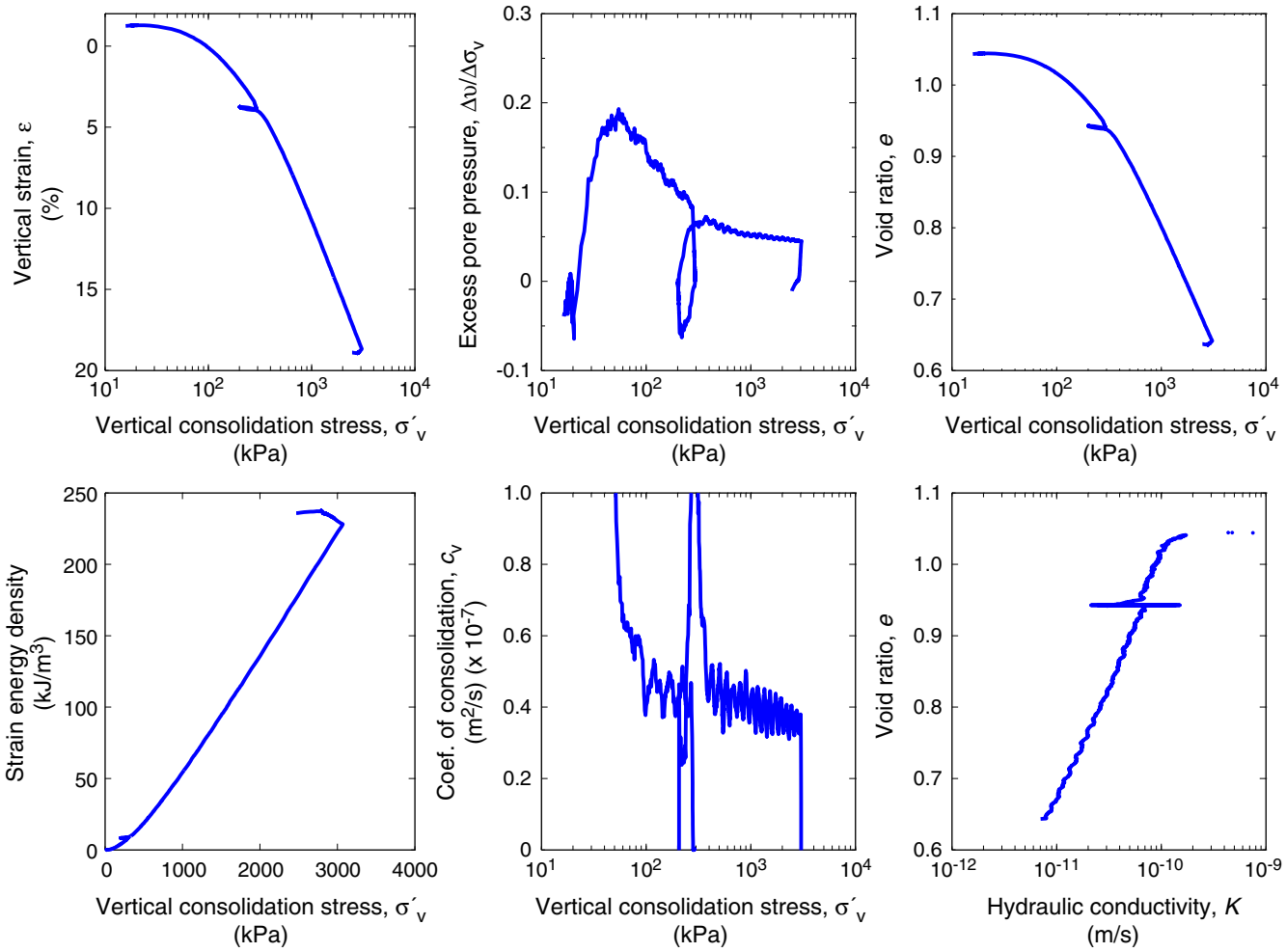

Figure F13. CRS808 consolidation data for Sample 308-U1322B-15H-1WR, 126.28 mbsf. Coef. = coefficient.

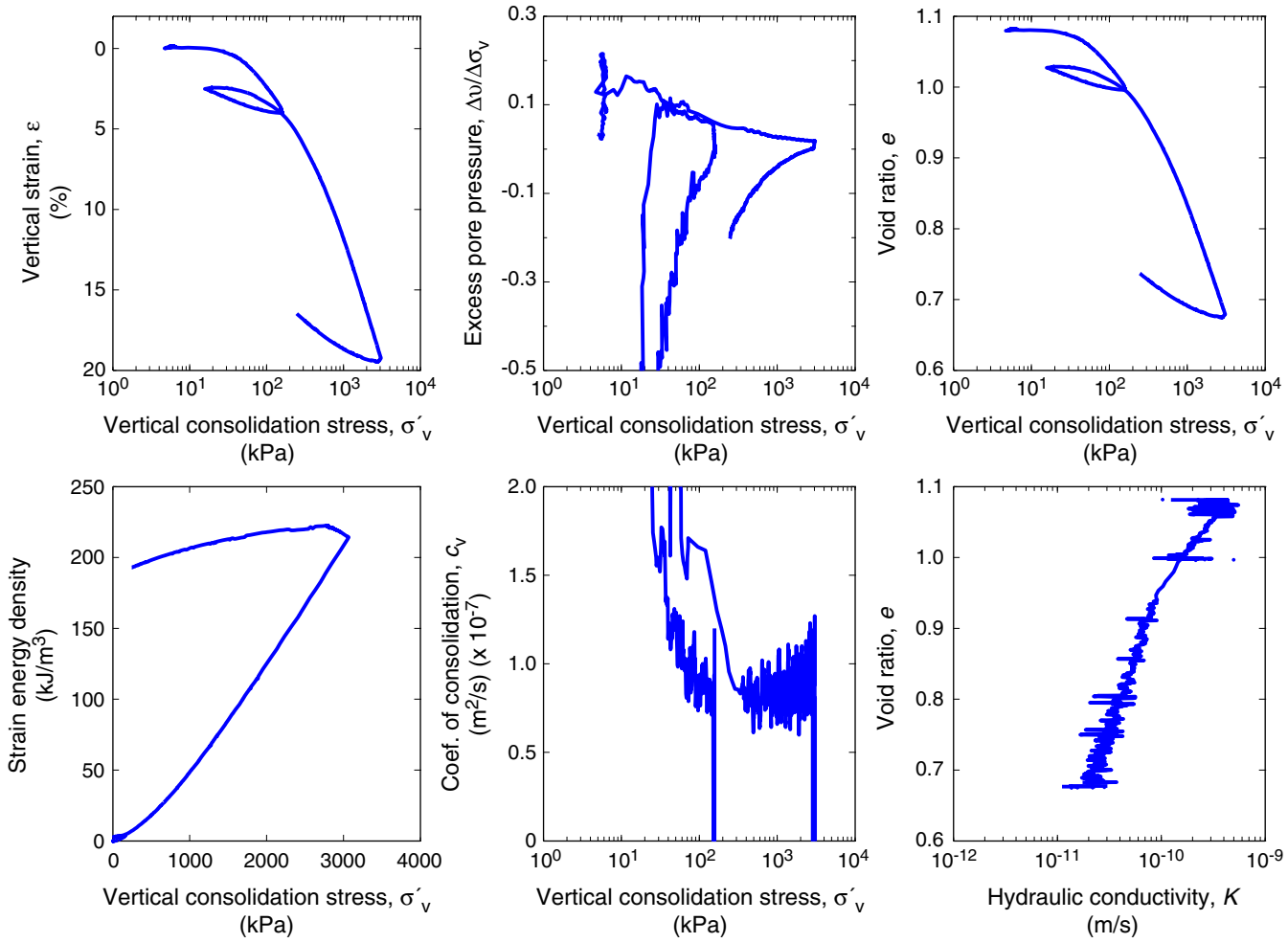

Figure F14. CRS810 consolidation data for Sample 308-U1322B-18H-6WR, 157.42 mbsf. Coef. = coefficient.

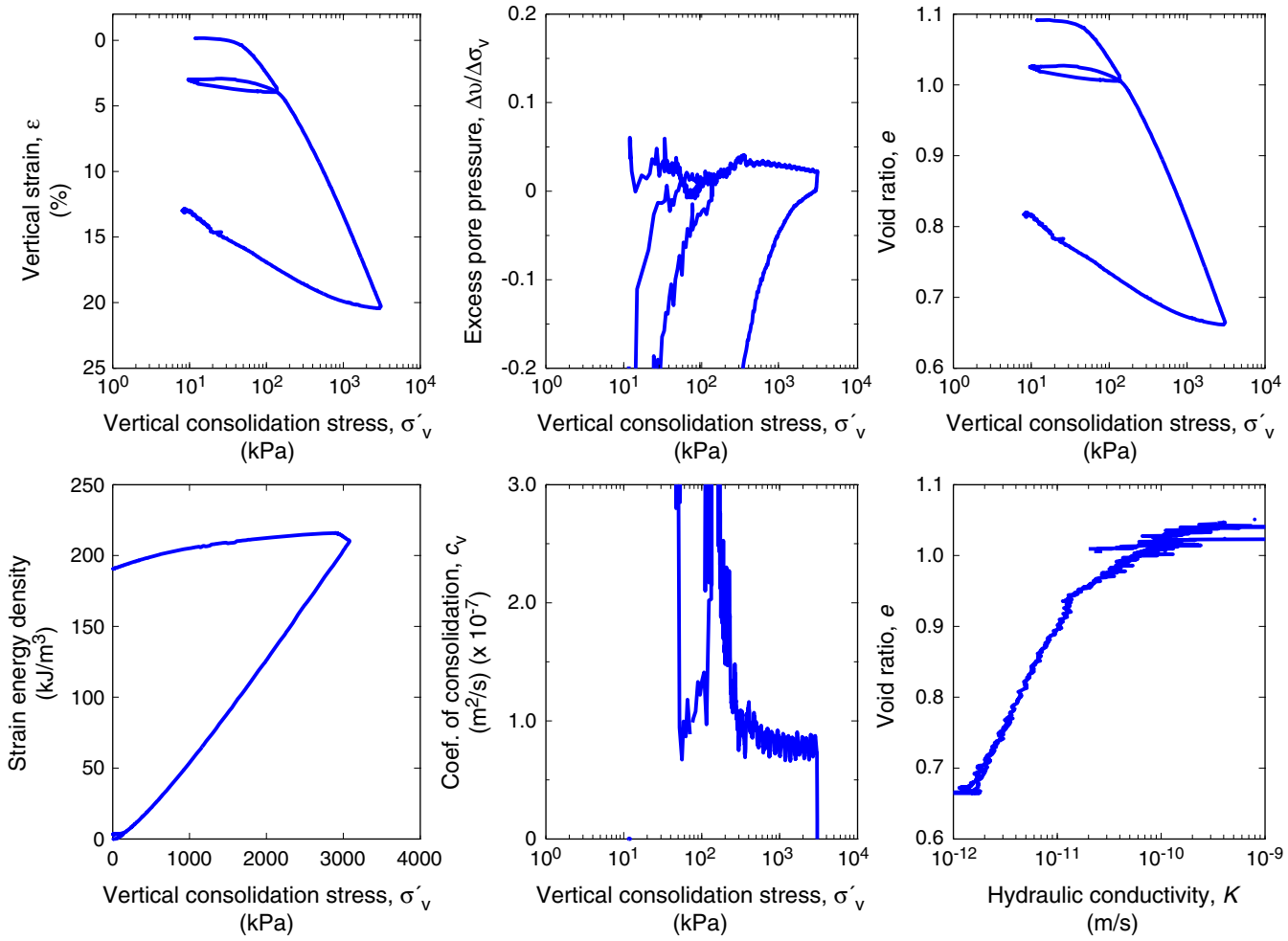

Figure F15. CRS812 consolidation data for Sample 308-U1324B-23H-5WR, 200 mbsf. Coef. = coefficient.

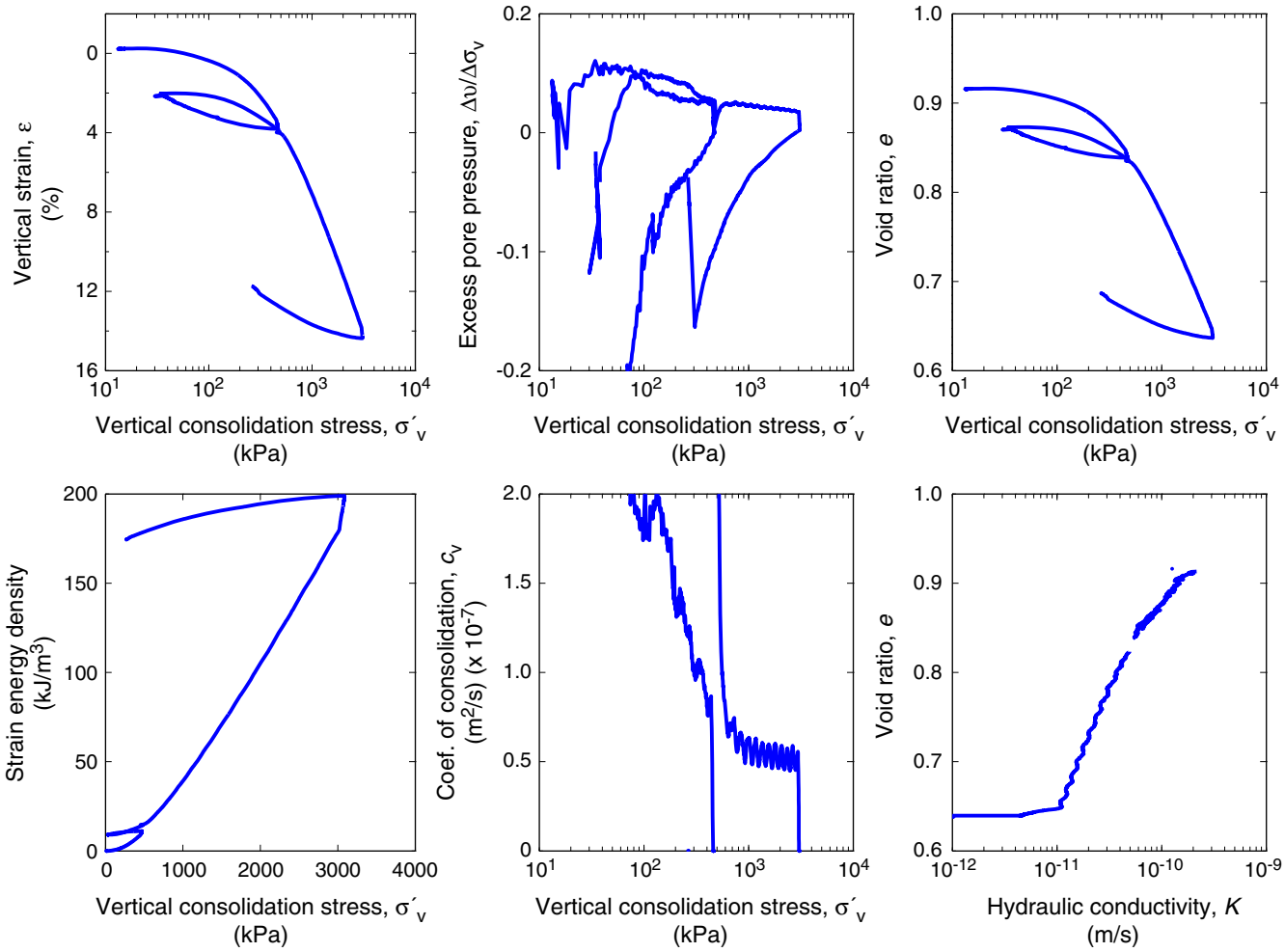

Figure F16. CRS813 consolidation data for Sample 308-U1324B-10H-7WR, 89.22 mbsf. Coef. = coefficient.

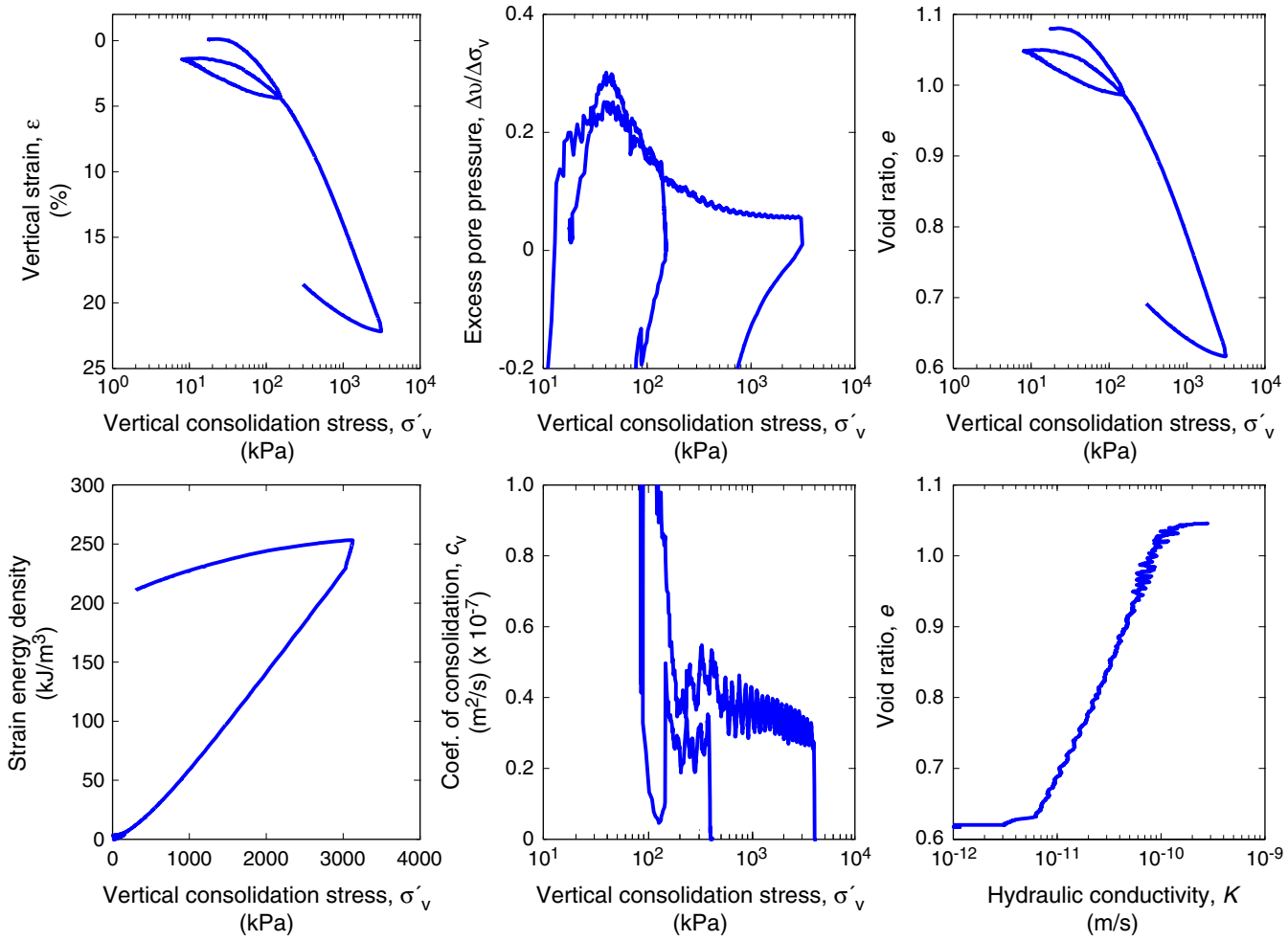

Figure F17. CRS815 consolidation data for Sample 308-U1322B-4H-3WR, 27.21 mbsf. Coef. = coefficient.

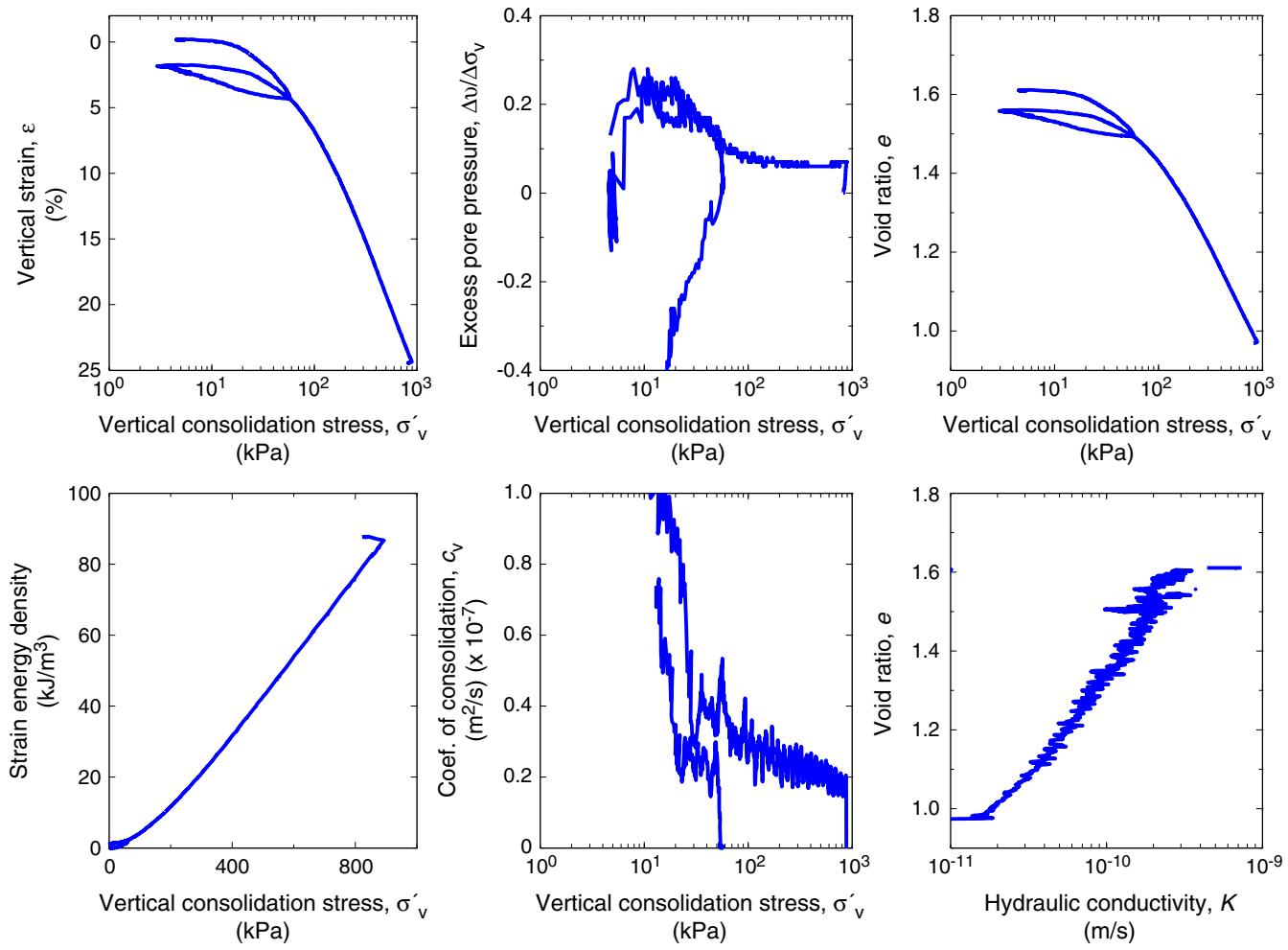

Figure F18. CRS824 consolidation data for Sample 308-U1322B-25H-6WR, 209.81 mbsf. Coef. = coefficient.

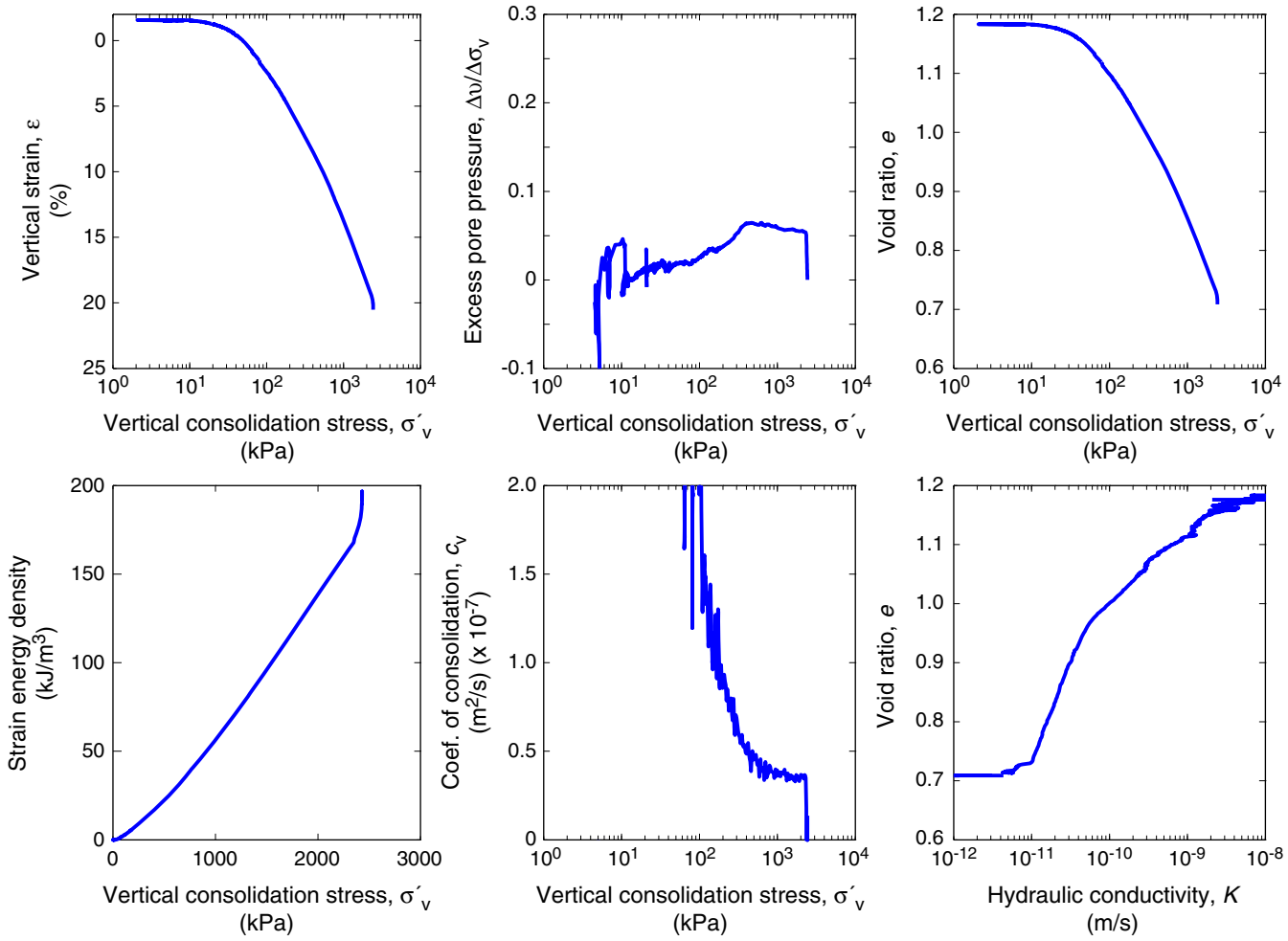

Figure F19. CRS825 consolidation data for Sample 308-U1322B-21H-3WR, 178.7 mbsf. Coef. = coefficient.

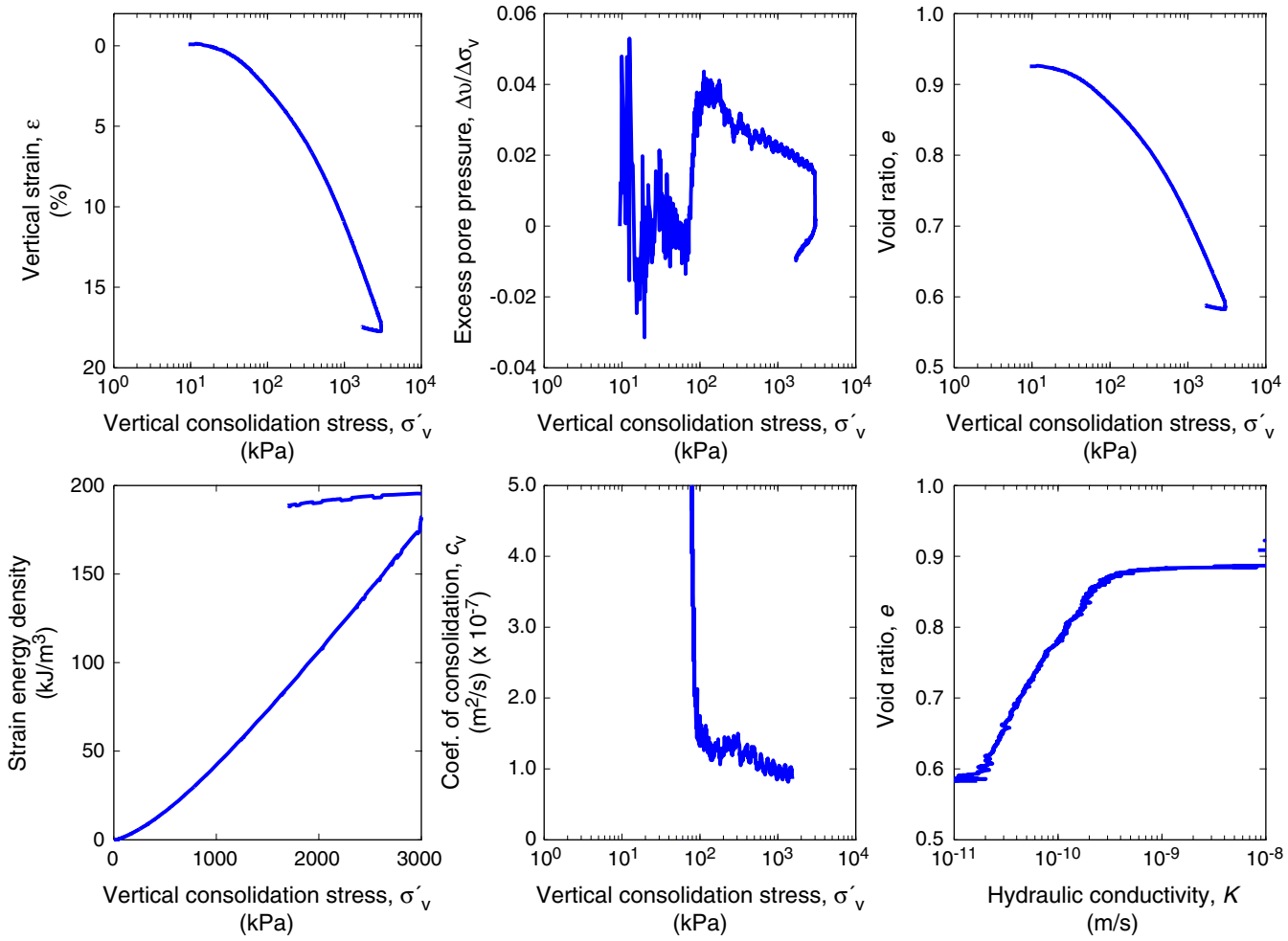

Figure F20. CRS826 consolidation data for Sample 308-U1322D-1H-2WR, 42.87 mbsf. Coef. = coefficient.

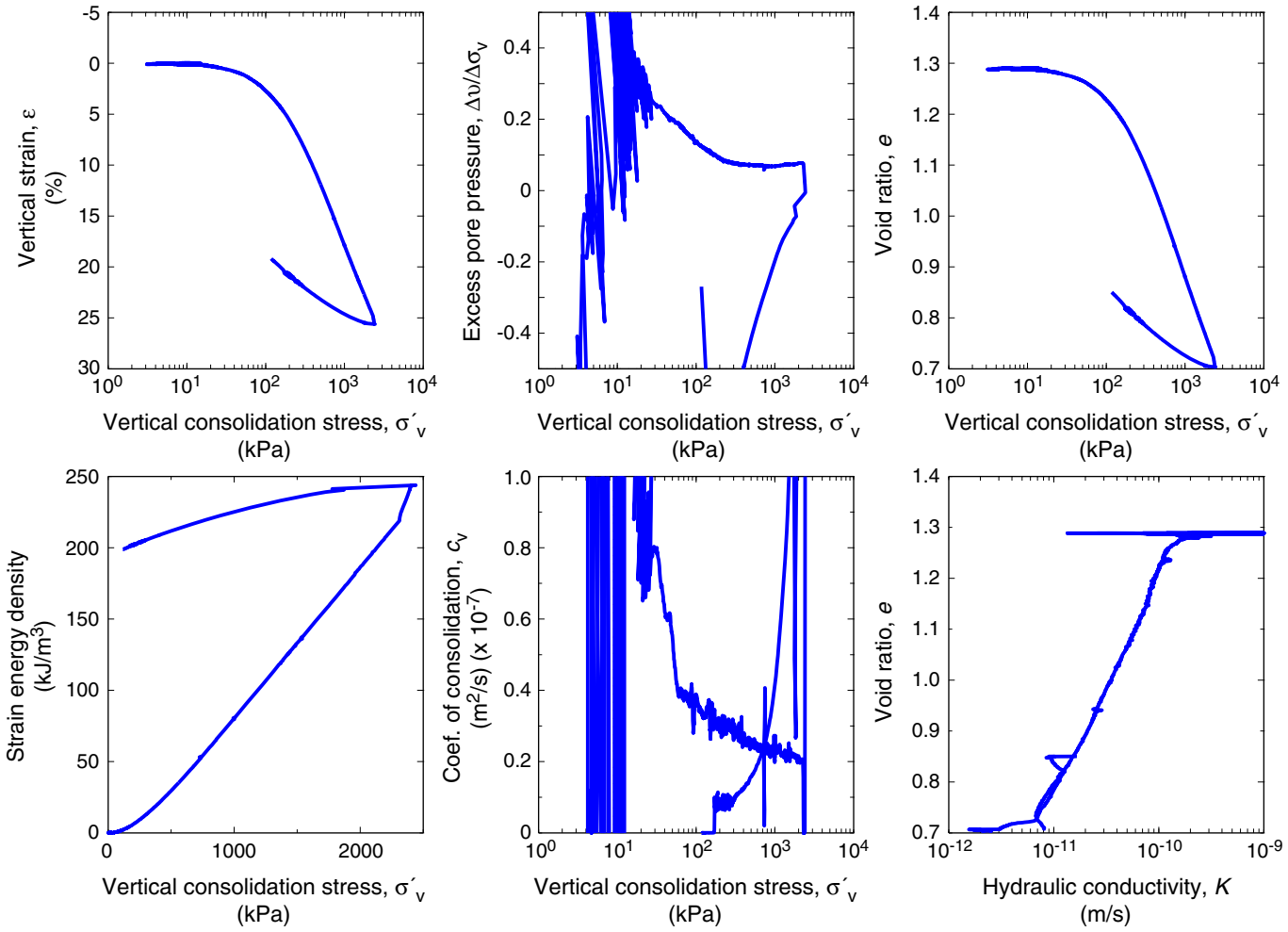

Figure F21. CRS001 consolidation data for Sample 308-U1324C-6H-3WR, 304.02 mbsf. Coef. = coefficient.

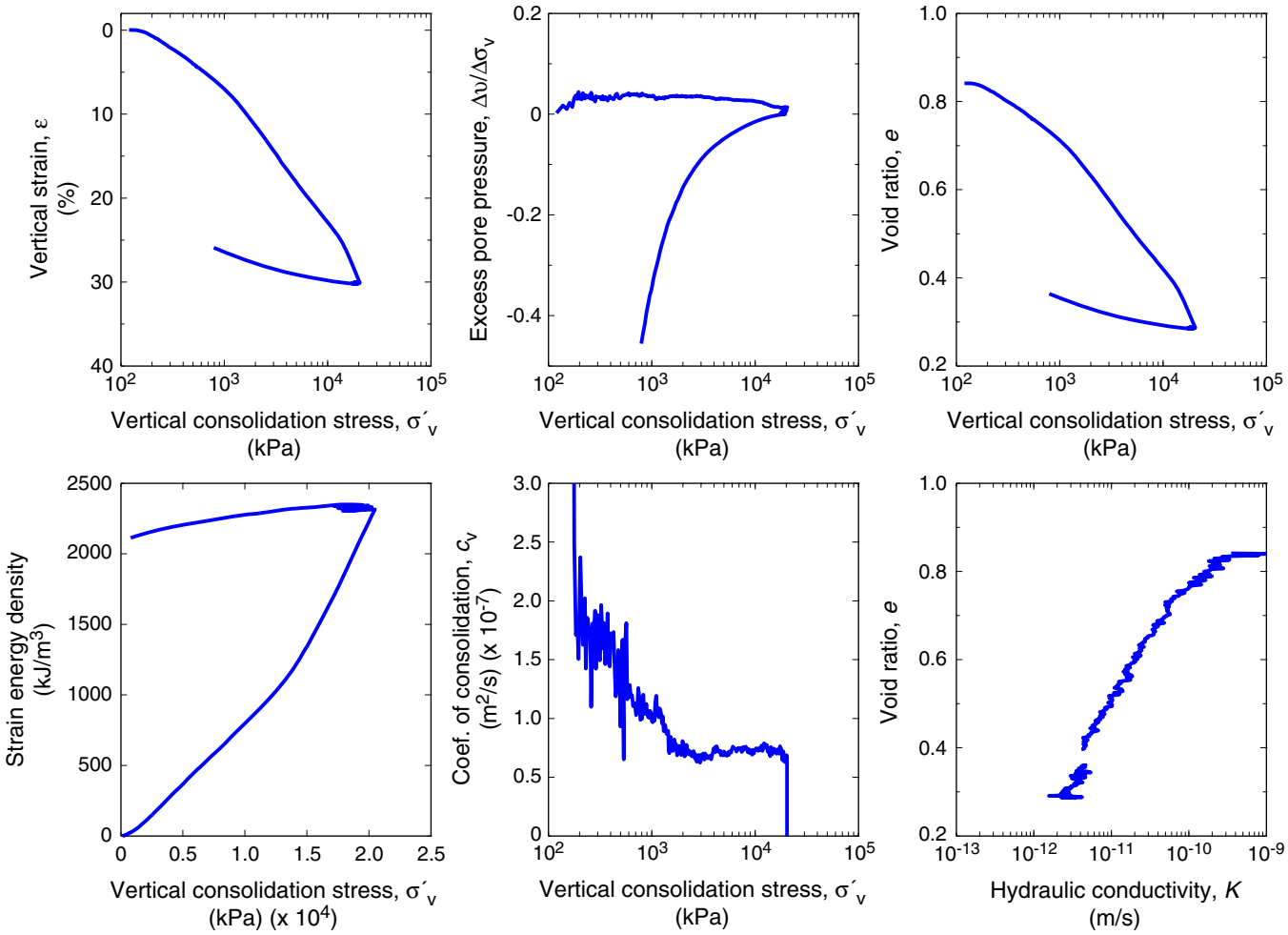

Figure F22. CRS002 consolidation data for Sample 308-U1324C-6H-3WR, 303.94 mbsf. Coef. = coefficient.

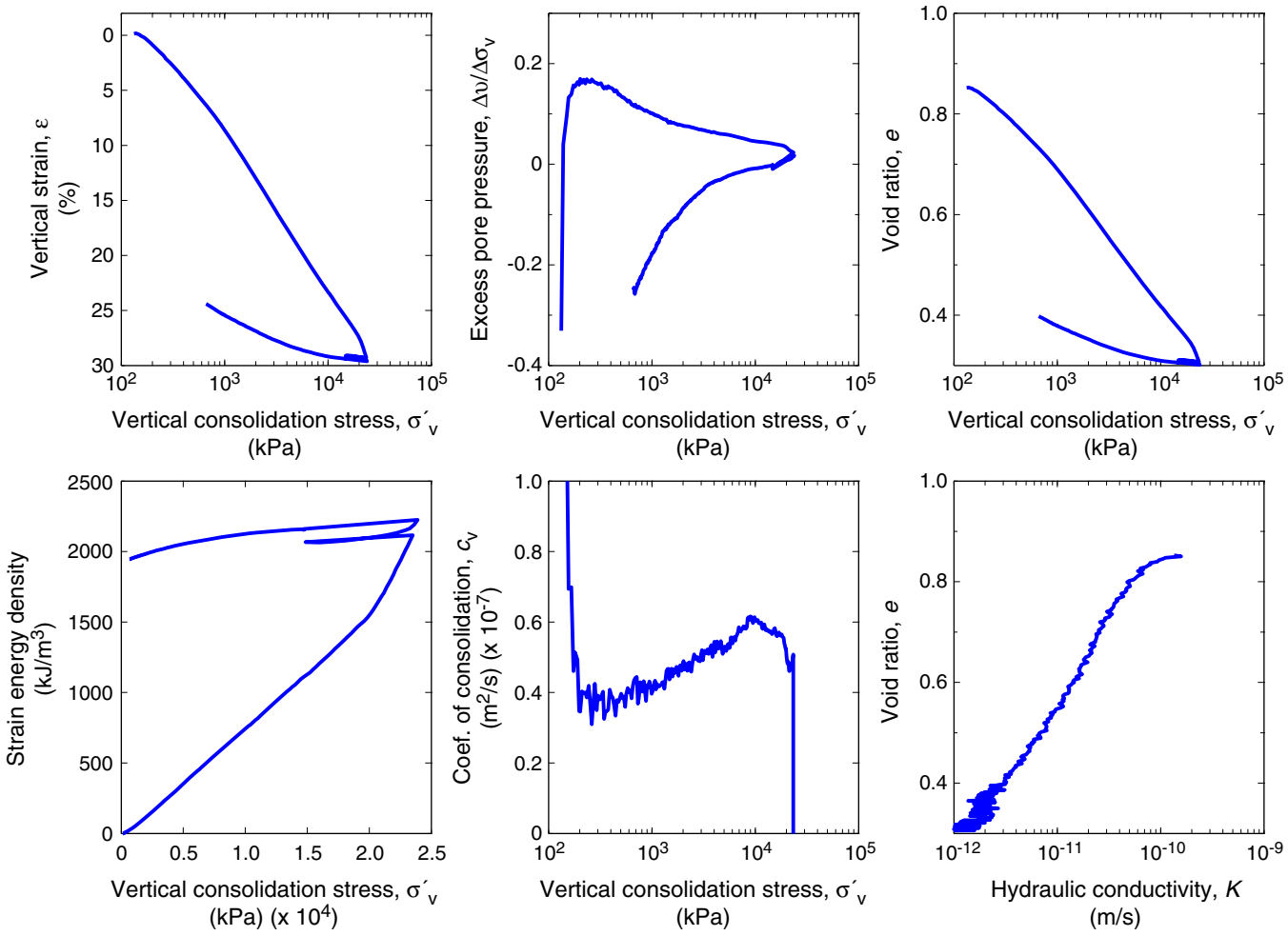

Figure F23. CRS003 consolidation data for Sample 308-U1324C-1H-1WR, 51.21 mbsf. Coef. = coefficient.

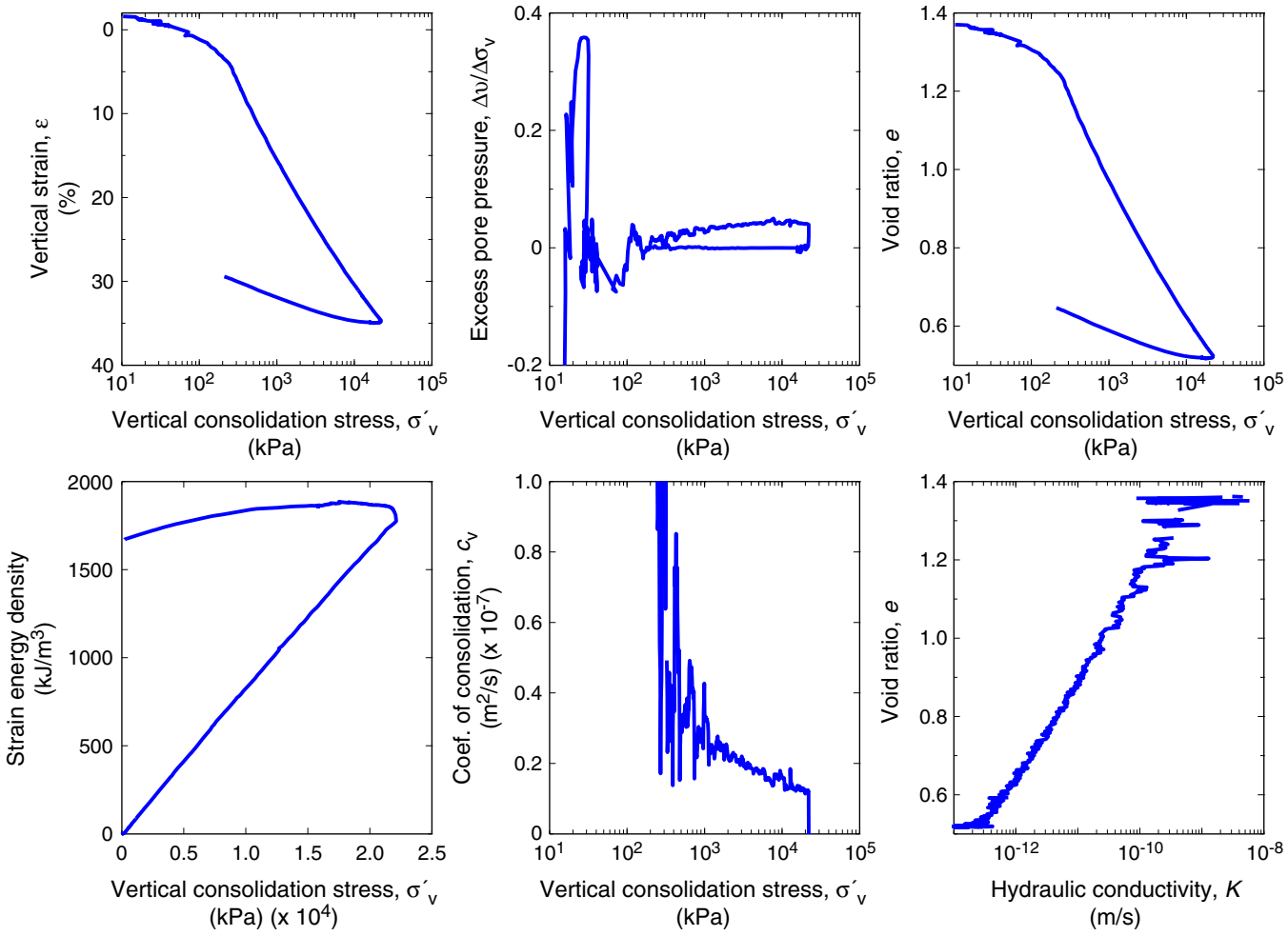

Figure F24. CRS004 consolidation data for Sample 308-U1324C-1H-1WR, 51.14 mbsf. Coef. = coefficient.

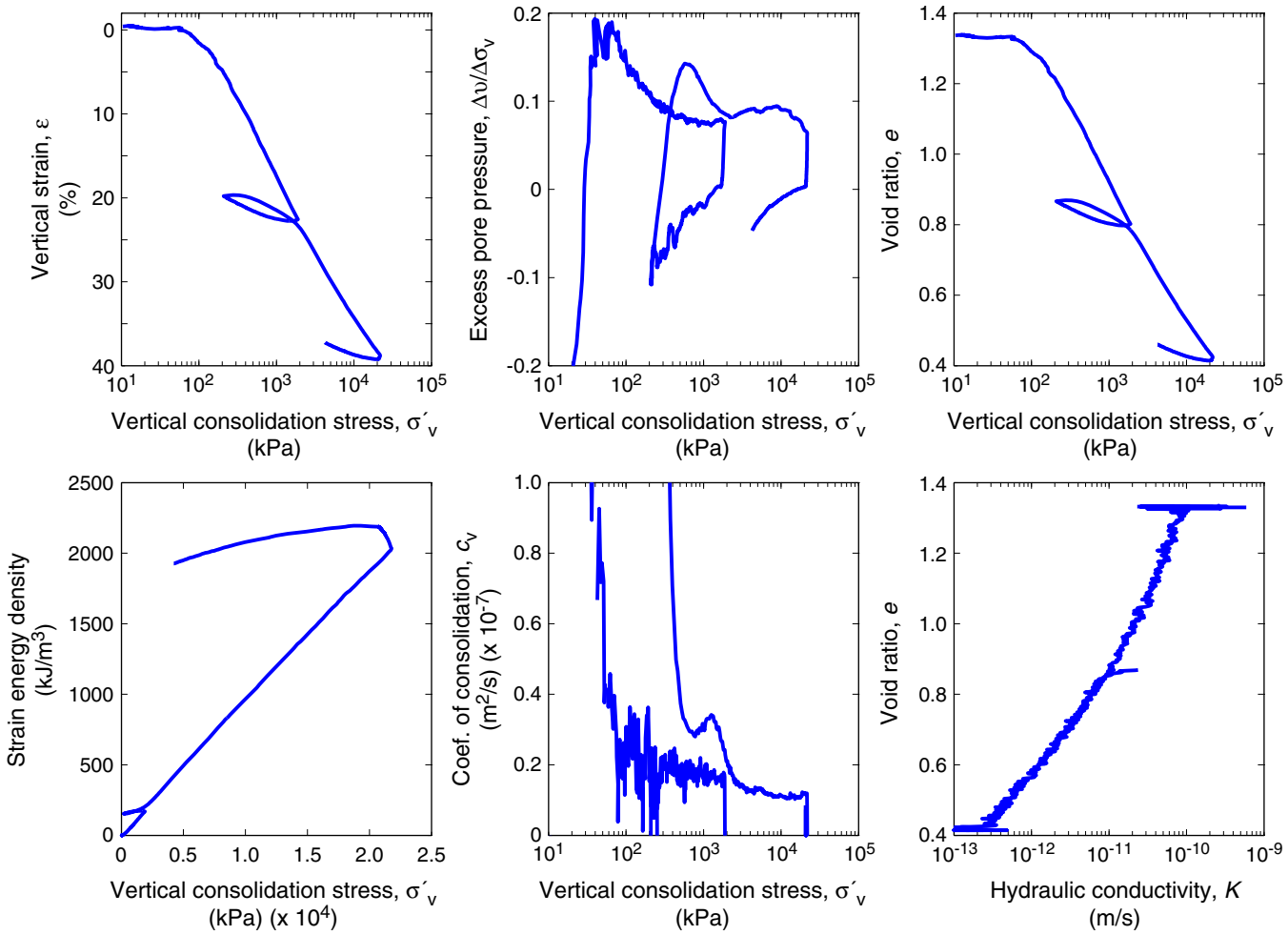

Figure F25. CRS005 consolidation data for Sample 308-U1324B-13H-7WR, 117.4 mbsf. Coef. = coefficient.

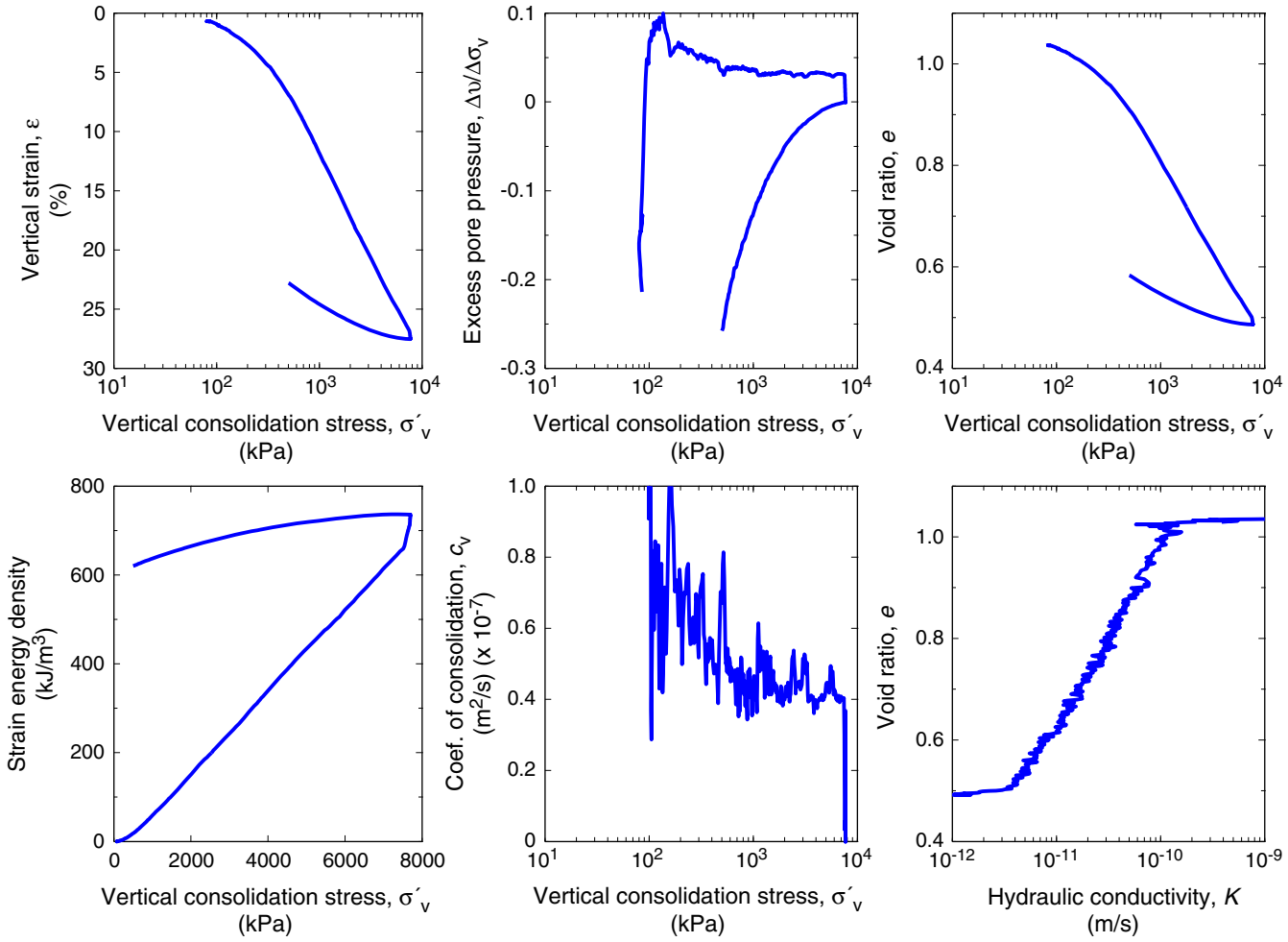

Figure F26. CRS006 consolidation data for Sample 308-U1324B-70X-6WR, 578.13 mbsf. Coef. = coefficient.

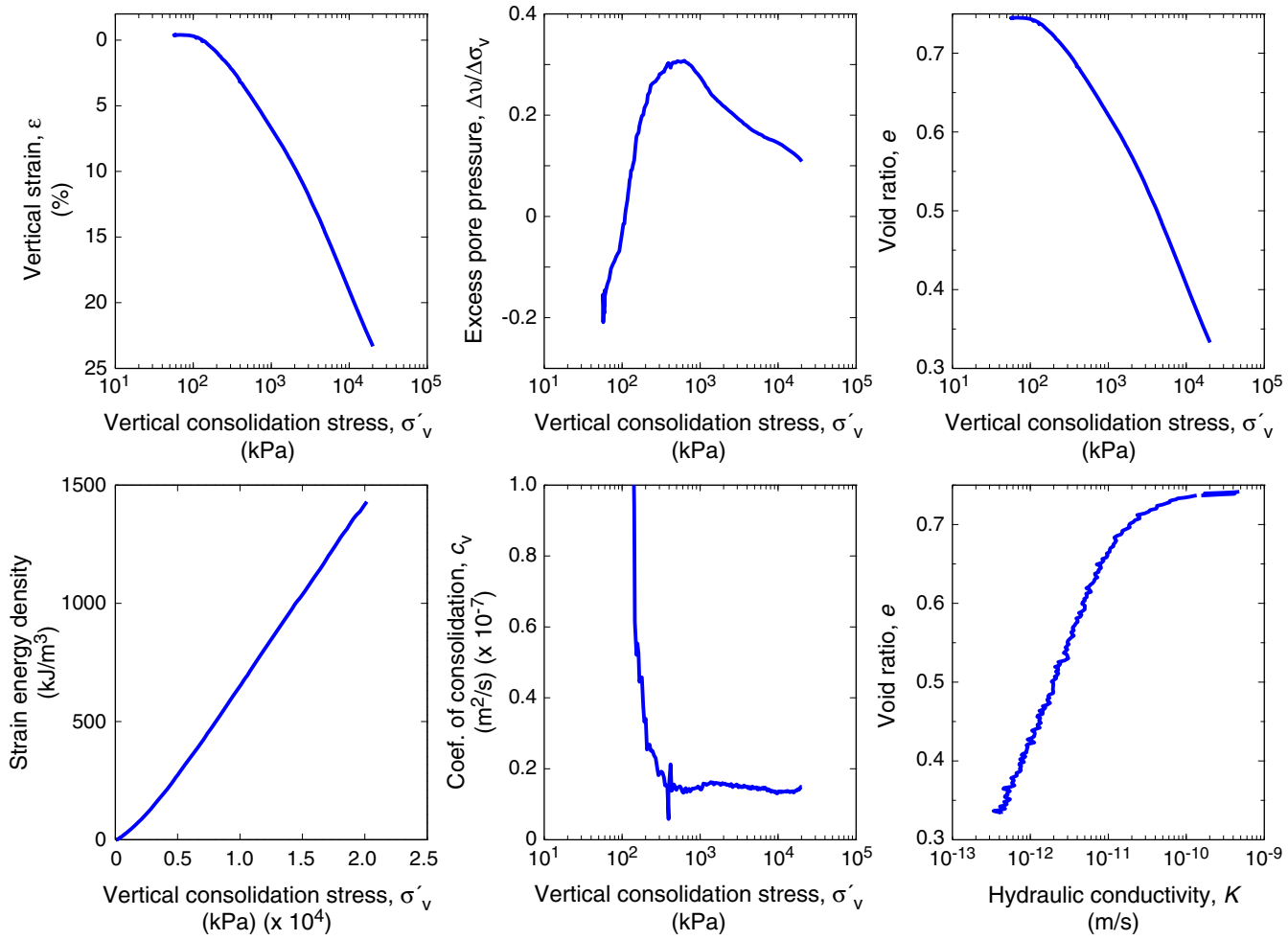

Figure F27. CRS007 consolidation data for Sample 308-U1324B-60X-2WR, 476.86 mbsf. Coef. = coefficient.

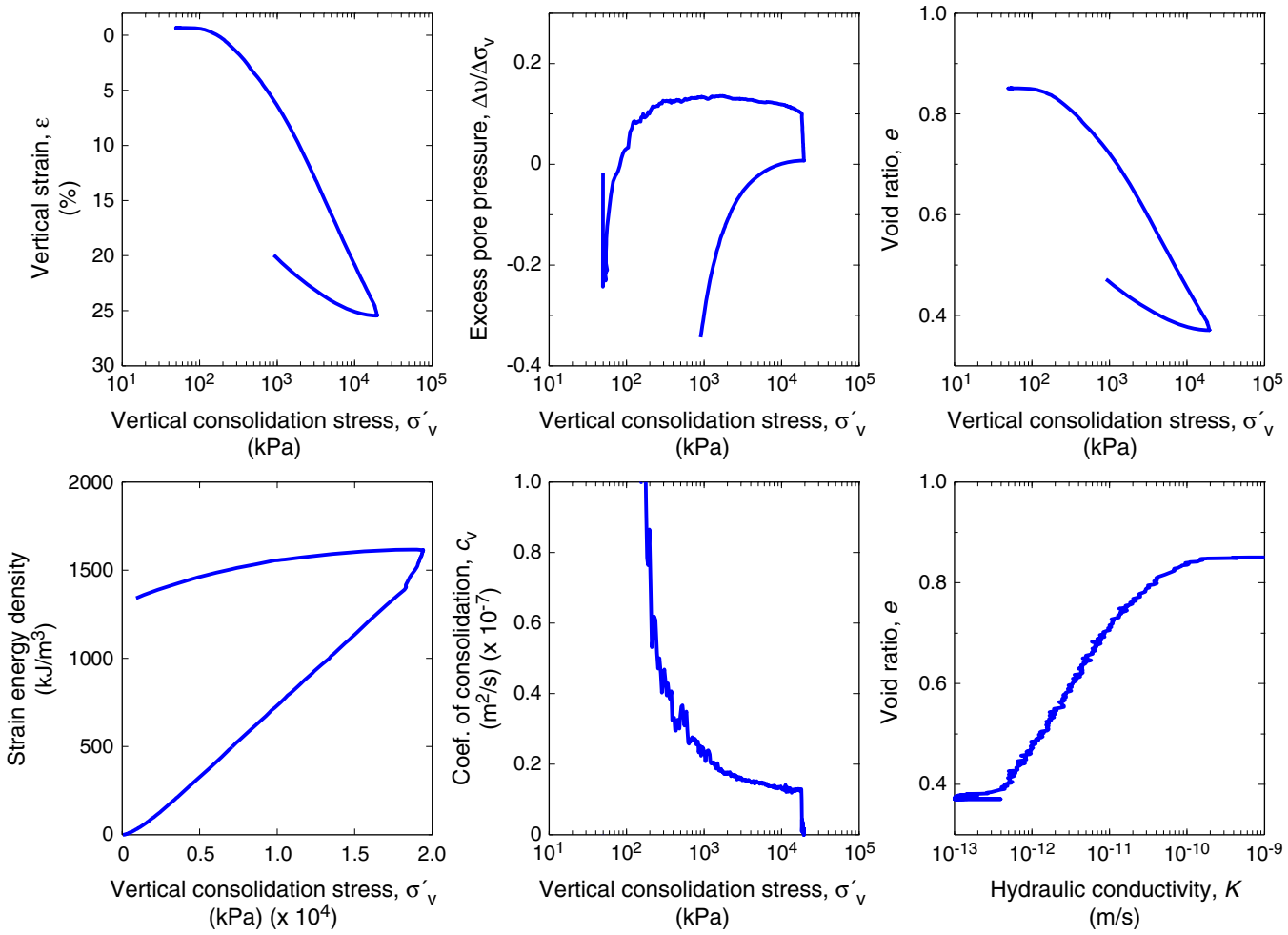

Figure F28. CRS008 consolidation data for Sample 308-U1324C-7H-1WR, 405.81 mbsf. Coef. = coefficient.

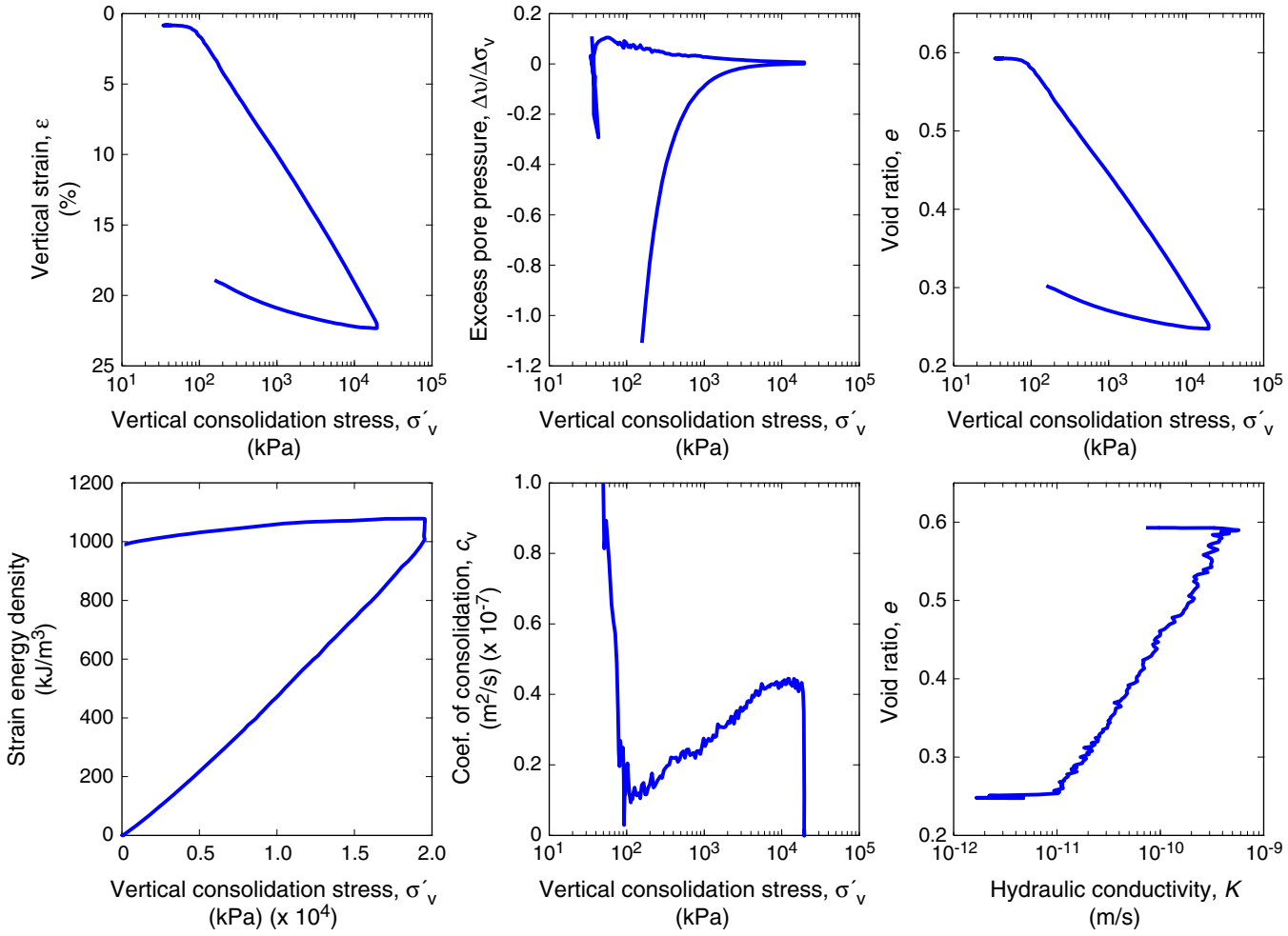

Figure F29. CRS013 consolidation data for Sample 308-U1324B-4H-7WR, 32.14 mbsf. Coef. = coefficient.

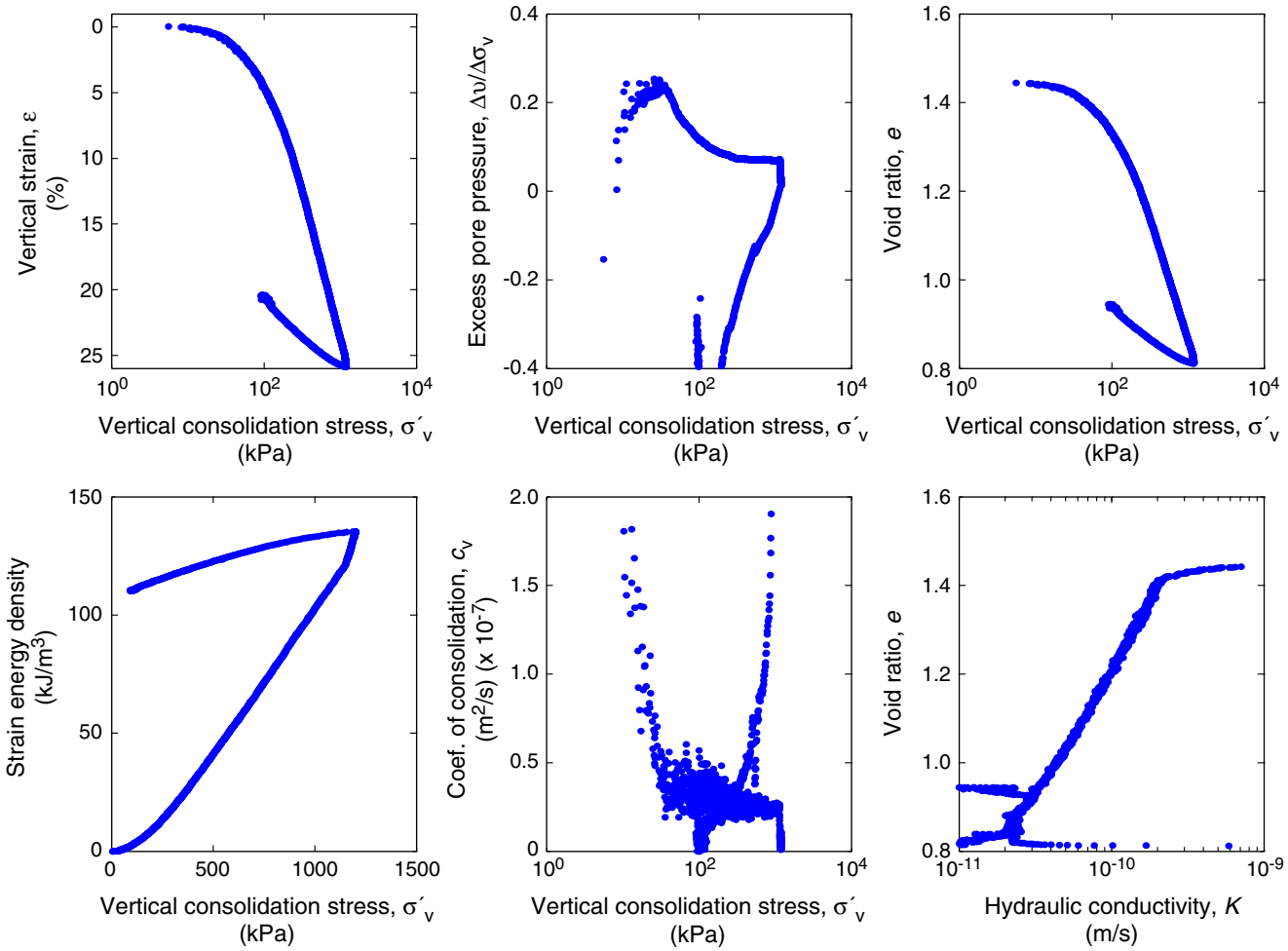

Figure F30. CRS014 consolidation data for Sample 308-U1324B-4H-7WR, 32.10 mbsf. Coef. = coefficient.

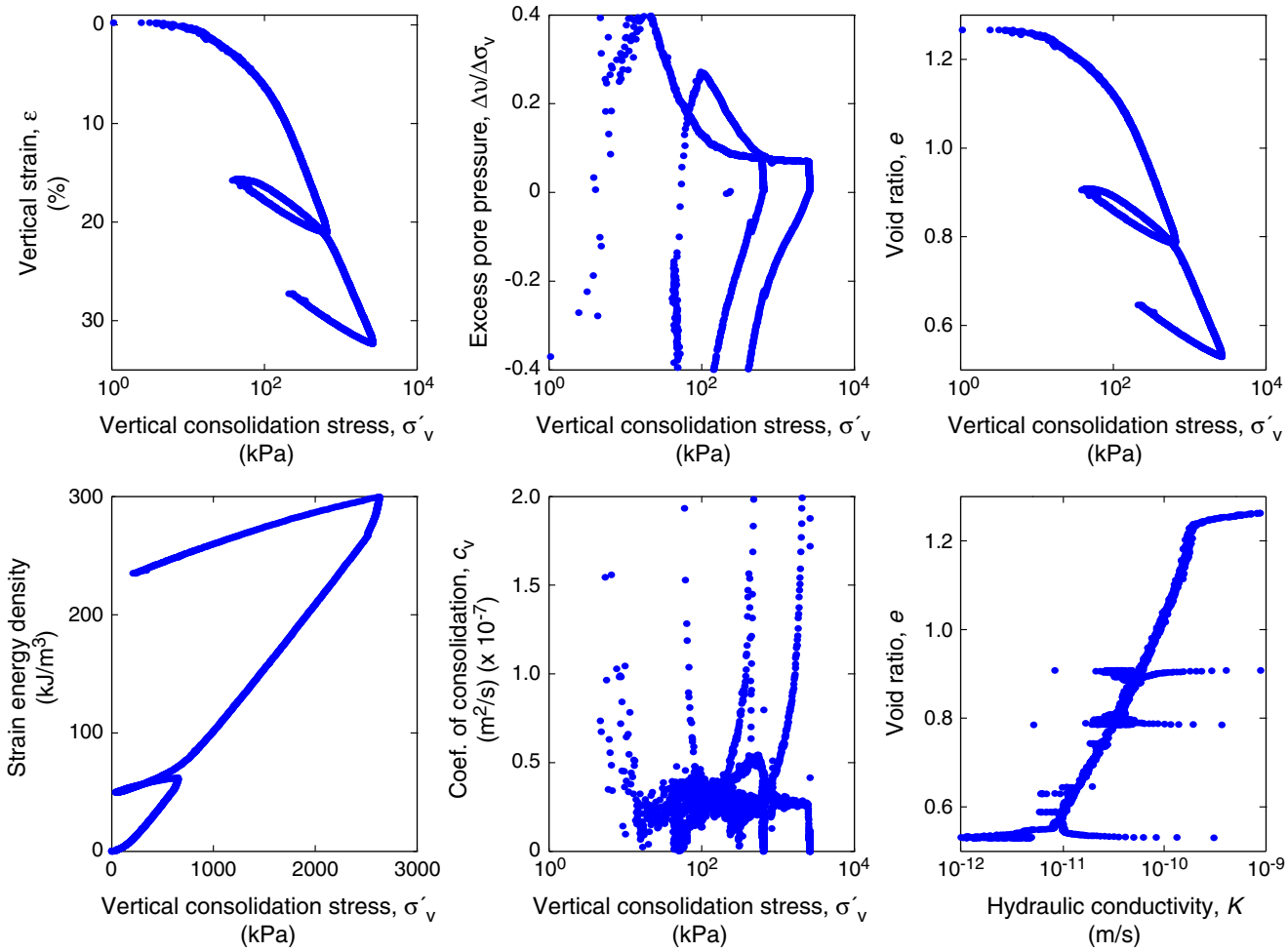

Figure F31. CRS015 consolidation data for Sample 308-U1324B-7H-7WR, 60.62 mbsf. Coef. = coefficient.

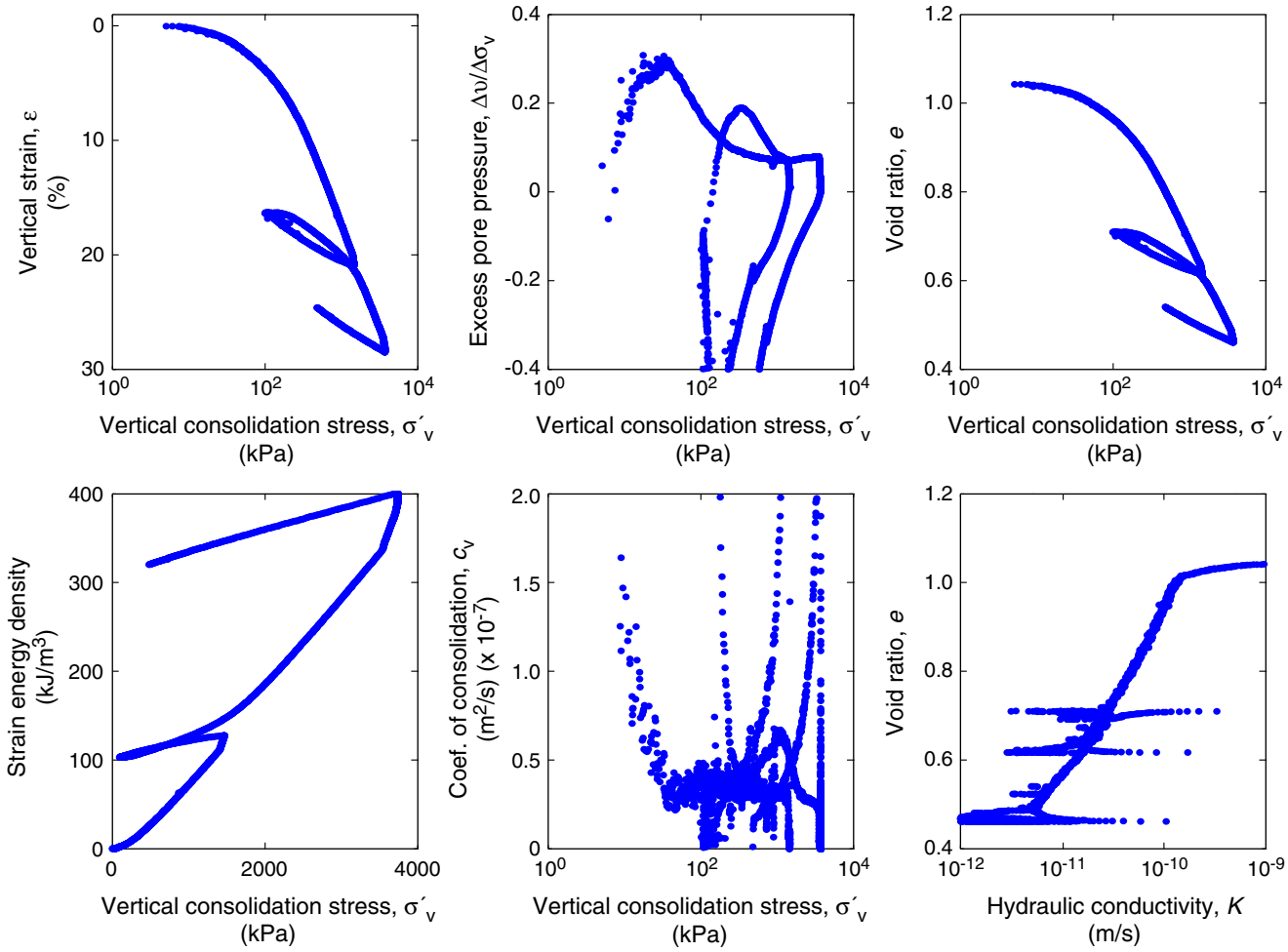

Figure F32. CRS018 consolidation data for Sample 308-U1324B-26H-3WR, 220.34 mbsf. Coef. = coefficient.

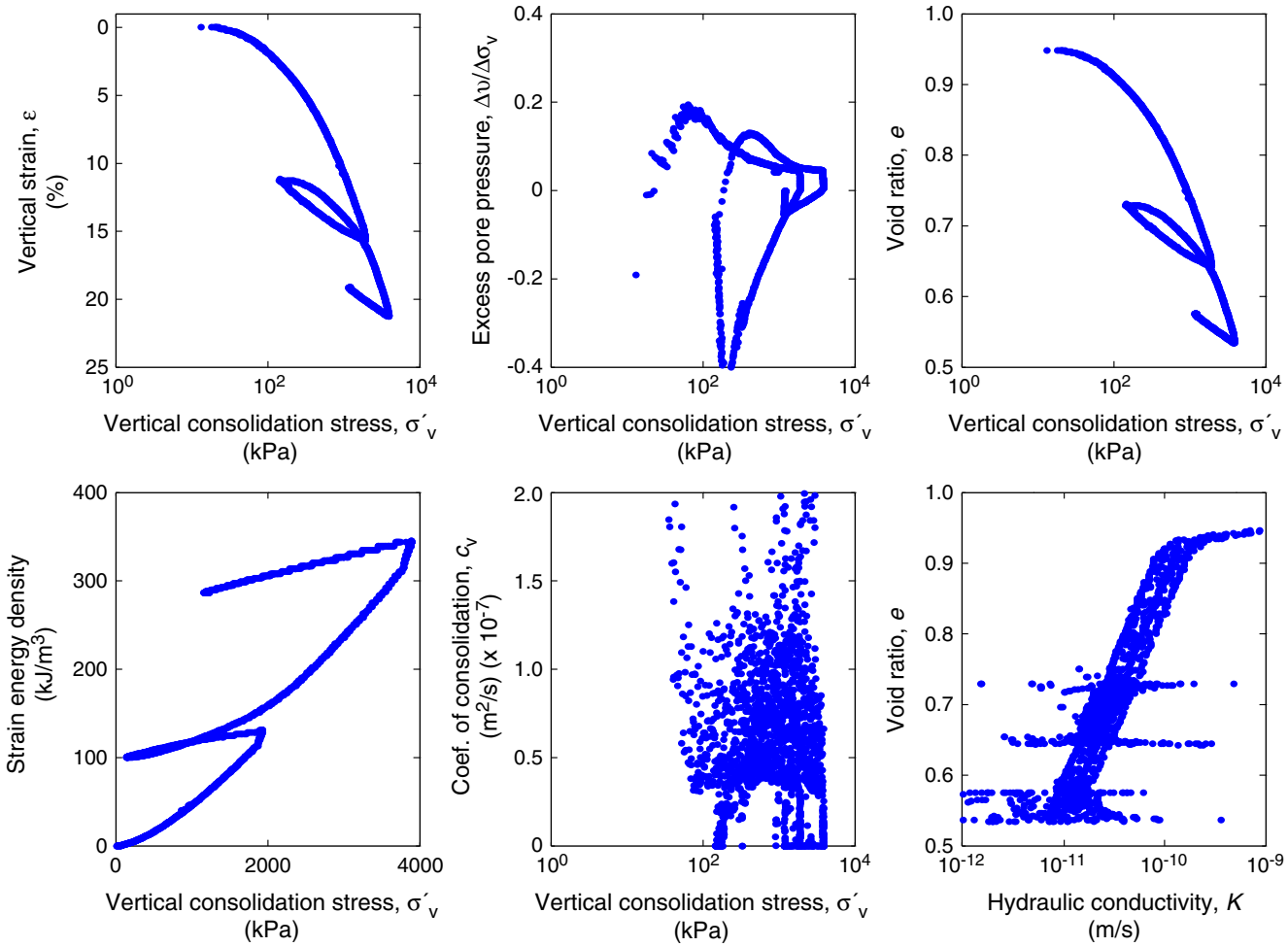

Figure F33. CRS019 consolidation data for Sample 308-U1324B-31H-3WR, 261.02 mbsf. Coef. = coefficient.

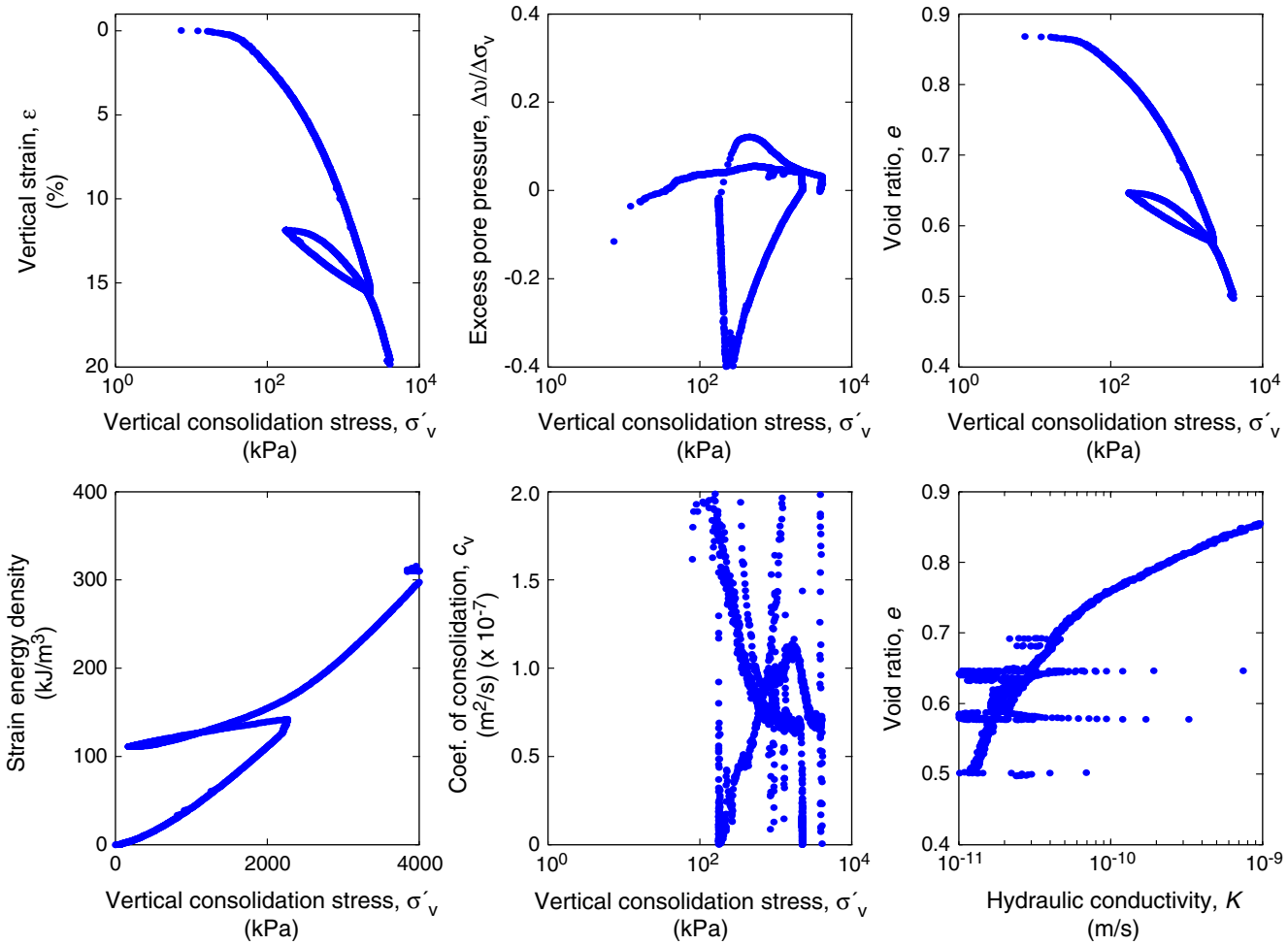

Figure F34. CRS020 consolidation data for Sample 308-U1324B-21H-3WR, 183.14 mbsf. Coef. = coefficient.

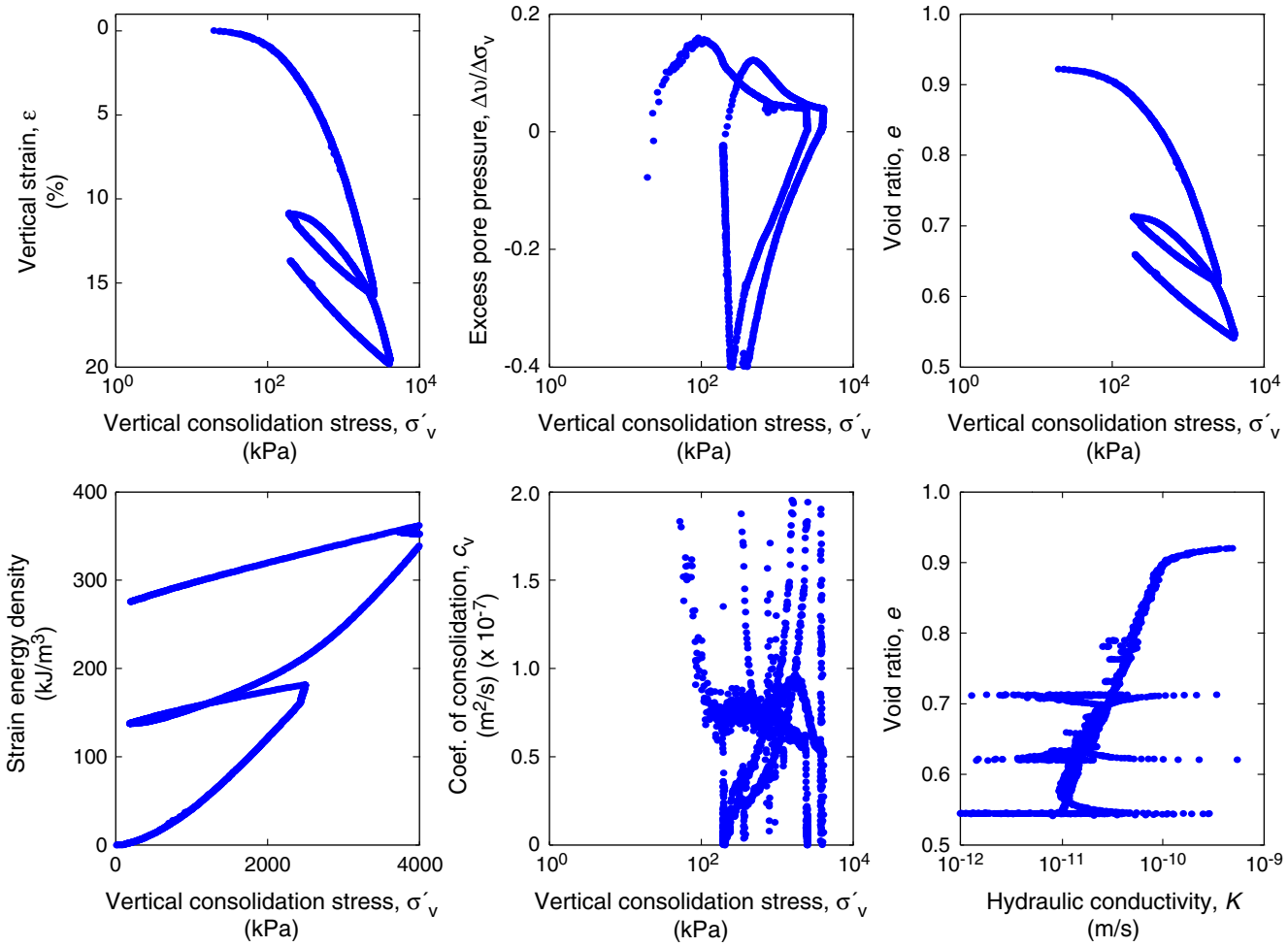

Figure F35. CRS021 consolidation data for Sample 308-U1322D-3H-3WR, 103.44 mbsf. Coef. = coefficient.

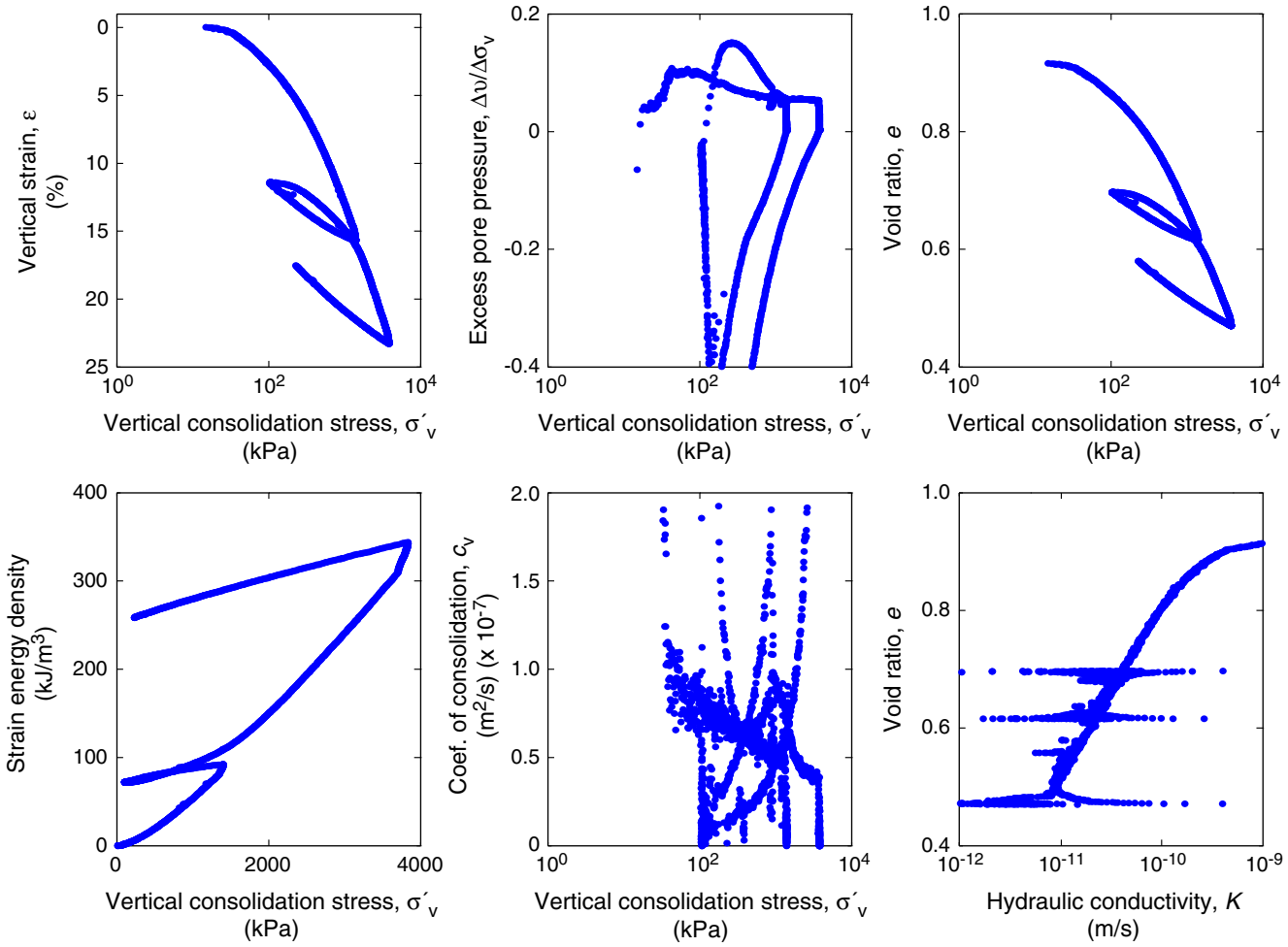

Figure F36. Compression and expansion indexes for Ursa Basin sediments (see Table T3).

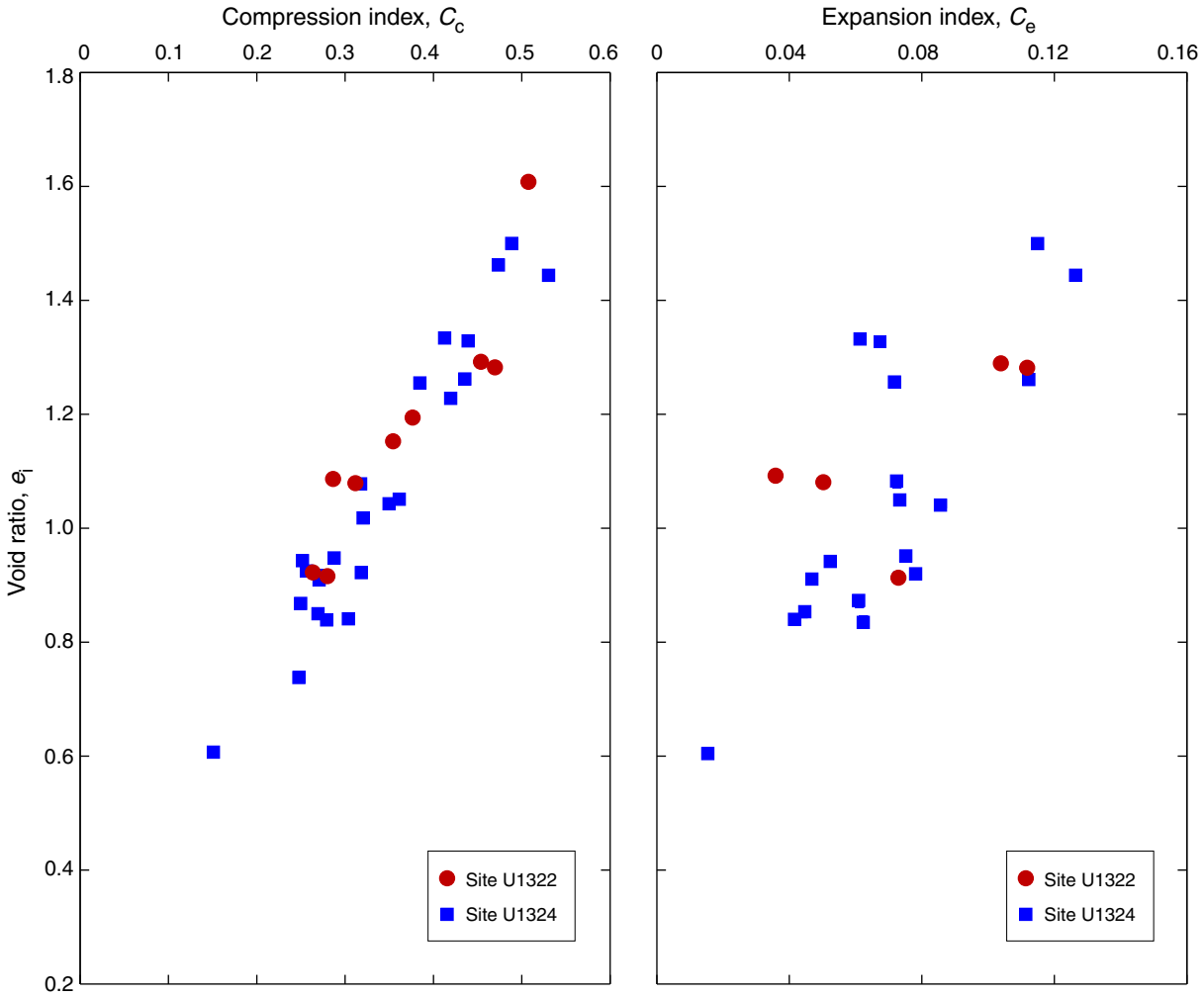

Figure F37. In situ hydraulic conductivity for Ursa Basin sediments (see Table T3).

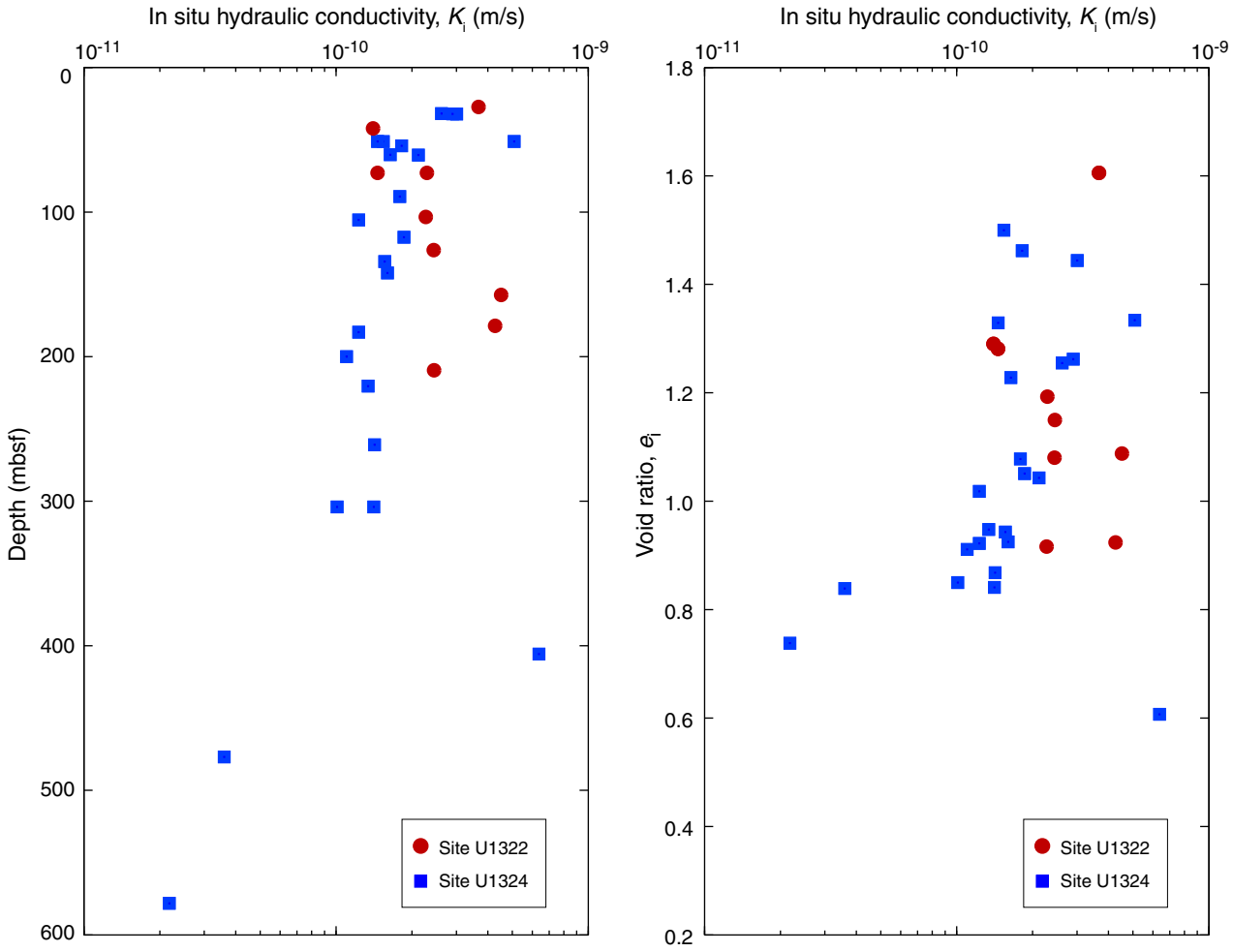

Figure F38. Coefficient of consolidation for Ursa Basin sediments (see Table T3).

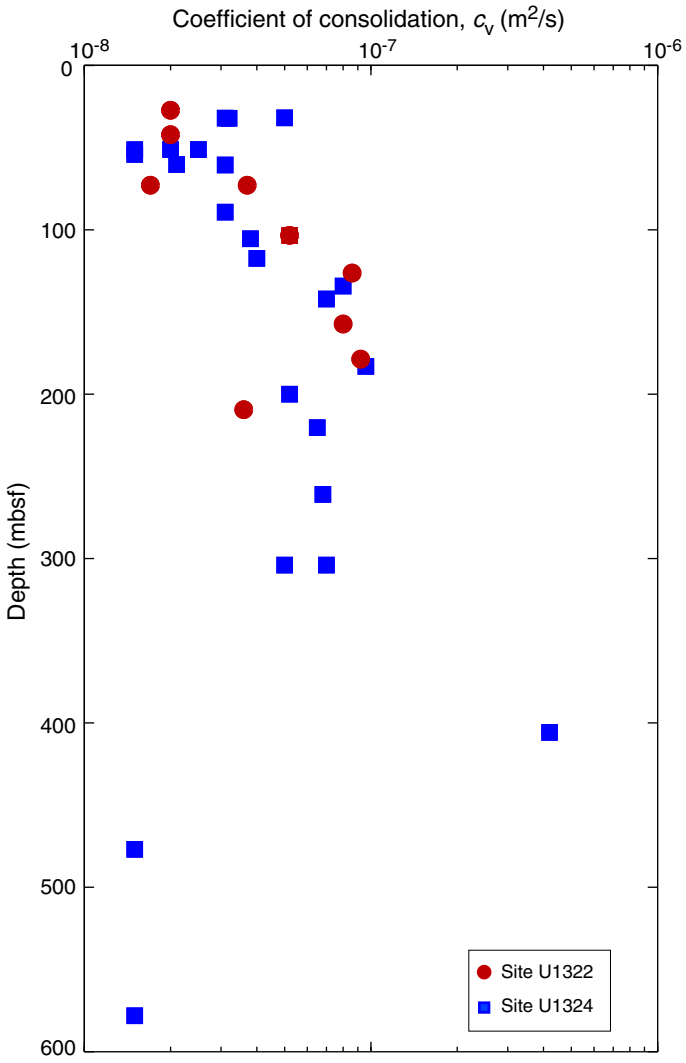

Figure F39. Preconsolidation pressure for Ursa sediments (see Table T3). Preconsolidation stress determined using work-stress method proposed by Becker et al. (1987). Hydrostatic vertical effective stress (σ'_{vh}) calculated using shipboard bulk density data assuming seawater density of 1.024 g/cm^3.

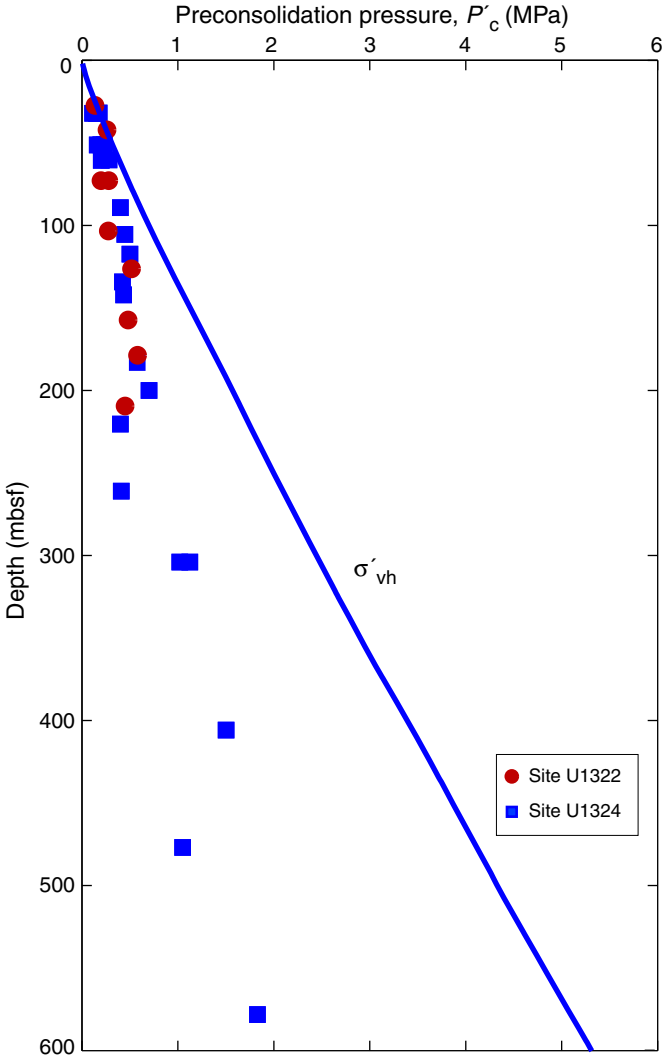

Table T1. Summary of tests conducted on Ursa Basin sediments. (**See table notes.**)

Core, section, interval (cm)	Depth (mbsf)	Cutting shoe	Index tests			CRSC		
			WC	PSA	X-ray	MIT	PSU	Rice
308-								
U1322B-4H-3WR, 117–137	27.17	Fugro	1	1	1	1		
U1322B-15H-1WR, 100–150	125.8	IODP-APC	1	1	1	1		
U1322B-18H-6WR, 0–40	157.3	Fugro	1	1	1	1		
U1322B-21H-3WR, 112–132	178.62	IODP-APC	1	1	1	1		
U1322B-25H-6WR, 97–147	209.5	IODP-APC	1	1	1	1		
U1322D-1H-2WR, 50–150	42	Fugro	1	1	1	1		
U1322D-2H-2WR, 50–150	72	Fugro	2	2	1	2		
U1322D-3H-3WR, 40–140	103.4	Fugro	1	1	1			1
U1324B-4H-7WR, 56–116	31.86	Fugro	3	2	2	1		2
U1324B-7H-7WR, 0–63	60.31	Fugro	2	2	2	1		1
U1324B-10H-7WR, 0–45	88.8	IODP-APC	1	1	1	1		
U1324B-13H-7WR, 15–35	117.24	Fugro	1	1			1	
U1324B-15H-5WR, 90–150	134.2	IODP-APCT	1	1	1	1		
U1324B-16H-5WR, 90–150	142.13	IODP-APC	1	1	1	1		
U1324B-21H-3WR, 112–132	183.12	Fugro	1	1	1			1
U1324B-23H-5WR, 0–22	199.8	Fugro	1	1	1	1		
U1324B-26H-3WR, 122–142	220.32	IODP-APC	1	1	1			1
U1324B-31H-3WR, 120–140	261	Fugro	1	1	1			1
U1324B-60X-2WR, 130–150	476.7	IODP-XCB	1	1			1	
U1324B-70X-6WR, 40–90	577.67	IODP-XCB	1	1			1	
U1324C-1H-1WR, 110–140	51.1	IODP-APC	4	4	1	2	2	
U1324C-2H-4WR, 0–100	104.5	Fugro	1	1	1	1		
U1324C-6H-3WR, 0–106	303	Fugro	2	2			2	
U1324C-7H-1WR, 50–150	405.5	IODP-APC	1	1			1	

Notes: See ODP *Technical Note* 31 (Graber et al., 2002) for coring system information and characteristics. WC = water content measurements, PSA = particle size analysis (**Sawyer et al.,** this volume). X-ray images in H. Nelson et al. (unpubl. data). CRSC = constant rate of strain consolidation. MIT = Massachusetts Institute of Technology, PSU = Pennsylvania State University, Rice = Rice University. IODP-APC = Integrated Ocean Drilling Program advanced piston coring system, IODP-XCB = IODP extended core barrel system, IODP-APCT = IODP advanced piston corer temperature tool.

Table T2. Nomenclature.

Variable	Definition	Dimension	SI unit
C_c	Compression index	Dimensionless	—
C_e	Expansion index	Dimensionless	—
G_s	Grain density	M/L^3	g/cm^3
H	Height of specimen	L	mm
H_0	Initial height of specimen	L	mm
K	Hydraulic conductivity	L/T	m/s
K_i	In situ hydraulic conductivity	L/T	m/s
OCR	Over consolidation ratio	Dimensionless	—
P'_c	Preconsolidation pressure	M/LT^2	kPa
SED	Strain energy density	M/LT^2	kJ/m^3
S_i	Initial saturation	Dimensionless	—
c_v	Coefficient of consolidation	L^2/T	m^2/s
e	Void ratio	Dimensionless	—
e_i	Initial void ratio measured on specimen	Dimensionless	—
k_i	In situ permeability	L^2	m^2
m_v	Frame compressibility	LT^2/M	1/kPa
u	Basal pore pressure	M/LT^2	kPa
u_b	Back pressure	M/LT^2	kPa
w_c	Water content measured on trimmings	Dimensionless	—
w_n	Water content measured on specimen	Dimensionless	—
Δu	Excess pore pressure	M/LT^2	kPa
$\Delta u/\sigma_v$	Normalized excess pore pressure	Dimensionless	—
$\delta\varepsilon/\delta t$	Strain rate	1/T	%/h
ε	Axial strain	Dimensionless	%
ε_i	Axial strain prior to compression	Dimensionless	%
ρ_b	Bulk density	M/L^3	g/cm^3
γ_w	Unit weight of water	M/L^2T^2	kN/m^3
σ_v	Applied vertical stress	M/LT^2	kPa
σ'_v	Vertical effective stress	M/LT^2	kPa
σ'_{iv}	Vertical effective stress prior to compression	M/LT^2	kPa
σ'_{vh}	Hydrostatic vertical effective stress	M/LT^2	kPa
σ'_{vm}	Maximum vertical effective stress during consolidation	M/LT^2	kPa

Table T3. CRSC test conditions and consolidation properties.

Test number	Hole, core, section	Depth (mbsf) Core top	Depth (mbsf) Specimen	Sample length (m)	Index test w_c (%)	Index test SD	Index test N	Specimen data w_n (%)	Specimen data ρ_b (kPa)	Specimen data e_i	Specimen data S_i (%)	Specimen data G_s (g/cm^3)	Test conditions u_b (kPa)	Test conditions σ'_{iv} (kPa)	Test conditions ε_i (%)	Test conditions $\delta\varepsilon/\delta t$ (%/h)	Test conditions $\Delta u/\sigma_v$ @ σ'_{vm} (%)	Consolidation properties C_c	Consolidation properties C_e	Consolidation properties P'_c (kPa)	Consolidation properties c_v (m^2/s)	Consolidation properties K_i (m/s)	Consolidation properties k_i (m^2)
CRS796	1322D-2H-2	72	72.78	0.78	46.3	0.8	2	47.25	1.795	1.281	102.6	2.78	384	2	0.05	0.25	13.5	0.4675	0.1114	280	1.7E–8	1.46E–10	1.46E–17
CRS797	1324C-1H-1	51.1	51.27	0.17	42.0	12.6	2	55.69	1.731	1.500	103.2	2.78	385	4	–0.06	0.27	12.0	0.4887	0.1144	160	1.5E–8	1.54E–10	1.54E–17
CRS798	1322D-2H-2	72	72.83	0.83	44.9	2.9	2	44.30	1.829	1.193	103.2	2.78	383	3	0.06	0.30	6.0	0.3762	—	200	3.7E–8	2.29E–10	2.29E–17
CRS799	1324C-1H-1	51.1	51.31	0.21	51.2	1.3	2	54.18	1.741	1.462	103.0	2.78	374	6	0.03	0.27	13.0	0.4736	—	224	1.5E–8	1.82E–10	1.82E–17
CRS800	1324B-4H-7	31.86	—	—	47.6	6.7	2	46.20	1.803	1.255	102.4	2.78	357	3	0.06	0.30	4.8	0.3846	0.0717	180	5.0E–8	2.62E–10	2.62E–17
CRS801	1324B-16H-5	142.13	—	—	33.3	0.5	2	33.77	1.932	0.925	101.5	2.78	379	3	0.00	0.26	3.0	0.2564	—	435	7.0E–8	1.60E–10	1.59E–17
CRS802	1324B-7H-7	60.31	—	—	44.6	1.8	2	44.42	1.802	1.228	100.6	2.78	349	3	0.04	0.31	11.0	0.4196	—	283	2.1E–8	1.64E–10	1.64E–17
CRS803	1324B-15H-5	134.2	—	—	31.8	0.0	2	34.99	1.932	0.943	103.2	2.78	378	10	–0.07	0.26	2.6	0.2517	0.0524	422	8.0E–8	1.56E–10	1.56E–17
CRS807	1324C-2H-4	104.5	105.48	0.98	37.3	0.1	2	35.89	1.872	1.018	98.0	2.78	410	16	–1.25	0.21	4.5	0.3204	—	448	3.8E–8	1.23E–10	1.23E–17
CRS808	1322B-15H-1	125.8	126.28	0.48	34.1	1.2	2	37.39	1.837	1.080	96.3	2.78	396	5	–0.07	0.20	1.7	0.3123	0.0500	516	8.6E–8	2.44E–10	2.44E–17
CRS810	1322B-18H-6	157.3	157.42	0.12	32.5	0.1	2	34.48	1.790	1.088	88.1	2.78	423	12	–0.15	0.21	2.2	0.2848	0.0359	480	8.0E–8	4.52E–10	4.52E–17
CRS812	1324B-23H-5	199.8	200	0.2	30.9	0.6	2	32.01	1.920	0.911	97.7	2.78	425	13	–0.23	0.20	3.5	0.2717	0.0470	700	5.2E–8	1.10E–10	1.10E–17
CRS813	1324B-10H-7	88.8	89.22	0.42	37.8	3.3	2	38.12	1.848	1.078	98.3	2.78	424	18	–0.09	0.21	5.6	0.3175	0.0725	400	3.1E–8	1.79E–10	1.79E–17
CRS815	1322B-4H-3	27.17	27.21	0.04	55.1	2.9	2	58.42	1.690	1.606	101.1	2.78	424	5	–0.16	0.18	7.0	0.5052	—	135	2.0E–8	3.67E–10	3.67E–17
CRS824	1322B-25H-6	209.5	209.81	0.31	32.8	0.6	3	34.50	1.739	1.150	83.4	2.78	384	5	–1.53	0.21	5.5	0.3544	—	450	3.6E–8	2.45E–10	2.45E–17
CRS825	1322B-21H-3	178.62	178.7	0.08	28.3	0.5	3	30.39	1.884	0.924	91.5	2.78	403	9	–0.09	0.16	1.8	0.2627	—	580	9.2E–8	4.27E–10	4.27E–17
CRS826	1322D-1H-2	42	42.87	0.87	44.6	1.8	3	45.21	1.763	1.29	97.4	2.78	387	5	0.05	0.21	7.5	0.455	0.1038	260	2.00E–8	1.40E–10	1.30E–17
CRS001	1324C-6H-3	303	304.02	1.02	31	0.20	4	—	—	0.84*		2.74	300	112	–0.03	0.42	2.5	0.3037	0.0421	1124	7.0E–8	1.41E–10	1.41E–17
CRS002	1324C-6H-3	303	303.94	0.94	32	1.40	3	—	—	0.85*		2.74	300	112	–0.14	0.60	4.0	0.2694	0.0442	1020	5.0E–8	1.01E–10	1.01E–17
CRS003	1324C-1H-1	51.1	51.21	0.11	50	1.80	3	—	—	1.33*		2.74	300	7	–1.59	0.15	4.0	0.4126	0.0365	197	2.5E–8	5.08E–10	5.08E–17
CRS004	1324C-1H-1	51.1	51.14	0.04	50	2.90	3	—	—	1.33*		2.74	299	8	–0.41	0.27	8.0	0.4393	0.0674	232	2.0E–8	1.46E–10	1.46E–17
CRS005	1324B-13H-7	117.24	117.4	0.16	40	1.40	3	39.700	1.867	1.05	101.60	2.74	300	80	0.69	0.27	3.0	0.3613	0.0734	500	4.0E–8	1.86E–10	1.86E–17
CRS006	1324B-70X-6	577.67	578.13	0.46	26	0.60	2	28.000	2.018	0.74	102.10	2.74	320	50	–0.38	0.45	11.0	0.2478	—	1829	1.5E–8	2.18E–11	2.18E–18
CRS007	1324B-60X-2	476.7	476.86	0.16	30	0.70	3	30.600	1.946	0.84	98.00	2.74	320	50	–0.66	0.36	11.0	0.2791	0.0624	1050	1.5E–8	3.60E–11	3.60E–18
CRS008	1324C-7H-1	405.5	405.81	0.31	23	0.60	3	19.900	2.040	0.61	87.90	2.74	300	40	0.84	0.60	1.0	0.1508	0.0153	1502	4.2E–7	6.38E–10	6.38E–17
CRS013	1324B-4H-7	31.86	32.14	0.84	48.1	0.3	4	53.55	1.697	1.444	100.16	2.7	387	6	–0.03	0.30	6.59	0.5303	0.1267	154	3.2E–8	3.01E–10	3.01E–17
CRS014	1324B-4H-7	31.86	32.10	0.80	45.4	1.3	4	47.18	1.757	1.262	100.93	2.7	386	2	–0.19	0.30	5.81	0.4355	0.1123	112	3.1E–8	2.90E–10	2.90E–17
CRS015	1324B-7H-7	60.31	60.62	0.31	39.8	6.4	4	39.04	1.837	1.043	101.05	2.7	387	1	0.00	0.30	7.31	0.3498	0.0862	202	3.1E–8	2.12E–10	2.12E–17
CRS018	1324B-26H-3	220.32	220.34	1.24	34.4	0.4	4	34.86	1.869	0.948	99.24	2.7	386	13	0.00	0.30	4.31	0.2875	0.0749	400	6.5E–8	1.34E–10	1.34E–17
CRS019	1324B-31H-3	261	261.02	1.22	29.6	0.1	4	26.46	1.871	0.868	91.65	2.7	387	7	–0.01	0.30	2.96	0.2497	0.0612	410	6.8E–8	1.42E–10	1.42E–17
CRS020	1324B-21H-3	183.12	183.14	1.14	32.9	1.6	4	34.09	1.884	0.922	99.84	2.7	387	20	–0.01	0.30	2.41	0.3183	0.0777	576	9.6E–8	1.23E–10	1.23E–17
CRS021	1322D-3H-3	103.4	103.44	0.44	31.7	1.0	4	32.91	1.873	0.916	97.03	2.7	387	15	0.00	0.30	4.52	0.2749	0.0727	274	5.2E–8	2.27E–10	2.27E–17

Notes: All sections taken from whole rounds. See Table T2 for variable definitions. SD = standard deviation, N = number of observations. * = water content not measured and e_i calculated from w_c assuming grain density of 2.74 g/cm^3. For other tests, e_i calculated from w_n assuming grain density of 2.74 g/cm^3 (Pennsylvania State University [PSU]), 2.78 g/cm^3 (Massachusetts Institute of Technology [MIT]), and 2.70 g/cm^3 (Rice University [Rice]). Tests CRS796–CRS826 performed at MIT, CRS01–CRS08 at PSU, and CRS13–CRS21 at Rice.

Table T4. Consolidation data file headers.

Time (s)	e (%)	σ_v (kPa)	u (kPa)	u_b (kPa)	σ'_v (kPa)	e	Δu (kPa)	K (m/s)	c_v (m^2/s)	$\Delta u/\sigma_v$	SED (kJ/m^3)
154750	–0.0302	120.169	281.752	299	120.001	0.8415	0.252	0.00E+00	0.00E+00	0.0021	0
155750	–0.0148	140.032	283.899	300	138.4327	0.8412	2.399	3.53E–10	1.29E–06	0.0171	0.0199
156740	0.0556	151.746	283.04	301	150.7193	0.8399	1.54	1.09E–09	1.40E–06	0.0101	0.1217
157750	0.1556	162.441	285.188	301	159.9823	0.8381	3.688	4.80E–10	5.22E–07	0.0227	0.2772
158740	0.2364	171.608	283.899	300	170.0087	0.8366	2.399	7.94E–10	7.49E–07	0.014	0.4107
159740	0.3493	181.794	287.335	301	177.904	0.8345	5.835	3.42E–10	2.49E–07	0.0321	0.6076
160750	0.4416	189.434	288.624	301	184.6847	0.8328	7.124	2.66E–10	1.71E–07	0.0376	0.7758
161740	0.5433	194.017	287.335	301	190.127	0.8309	5.835	3.23E–10	1.80E–07	0.0301	0.9671

Note: See Table T2 for variable definitions.